ABSTRACT

ASYMPTOTIC METHODS IN APPLIED WAVEGUIDE PROBLEMS

by
Helen Martynov

Some of the most challenging problems in acoustics and electromagnetics involve the study of scattered fields in waveguides caused by targets of elaborate shape. The complexity of the resulting scattered field depends on the geometry of the scatterer, and exact solutions exist only for the simple geometries.

The asymptotic methods developed in this dissertation give the approximate solutions for the scattered fields in two practically important geometries: an object placed inside a stratified waveguide, and a waveguide with multiple abrupt width transitions. The solutions for these geometries are obtained by approximating the field near the target or junction by the field that would be present if the waveguide walls were removed. This approximation is shown to be accurate if the waveguide width is large enough.

An asymptotic solution for the direct problem of scattering from the small object inside a stratified waveguide is obtained and investigated. Based on that approximation the solution to the problem of target localization for low frequency fields, or obstacles with certain symmetries, is developed. The solution of the shape reconstruction problem is demonstrated for an object in the high frequency limit.

An asymptotic solution for the direct problem of field scattering in the waveguide with multiple abrupt width transitions is also developed. Both Dirichlet and Neumann boundary conditions are considered. The applicability conditions of this approximation are investigated and the resulting accuracy is discussed. Numerical simulations supporting the validity of these asymptotic approximations are presented in each case.

ASYMPTOTIC METHODS IN APPLIED WAVEGUIDE PROBLEMS

by
Helen Martynov

A Dissertation
Submitted to the Faculty of
New Jersey Institute of Technology and
Rutgers, The State University of New Jersey - Newark
in Partial Fulfillment of the Requirements for the Degree of
Doctor of Philosophy in Mathematical Sciences

Department of Mathematical Sciences
Department of Mathematics and Computer Science, Rutgers-Newark

August 2001

APPROVAL PAGE

ASYMPTOTIC METHODS IN APPLIED WAVEGUIDE PROBLEMS

Helen Martynov

Gregory A. Kriegsmann, Ph.D, Dissertation Advisor — Date
Distinguished Professor, Department of Mathematical Sciences, NJIT

Jonathan H. C. Luke, Ph.D, Committee Member — Date
Associate Professor, Department of Mathematical Sciences, NJIT

David C. Stickler, Ph.D, Committee Member — Date
Professor, Department of Mathematical Sciences, NJIT

Peter G. Petropoulos, Ph.D, Committee Member — Date
Associate Professor, Department of Mathematical Sciences, NJIT

Edip Niver, Ph.D, Committee Member — Date
Associate Professor, Electrical and Computer Engineering Department, NJIT

BIOGRAPHICAL SKETCH

Author: Helen Martynov

Degree: Doctor of Philosophy

Date: August 2001

Undergraduate and Graduate Education:

- Doctor of Philosophy in Mathematical Sciences
  New Jersey Institute of Technology, Newark, NJ, 2001
- Master of Science in Electrical Engineering
  New Jersey Institute of Technology, Newark, NJ, 1993
- Bachelor of Science in Applied Mathematics
  Moscow Power Engineering Institute, Moscow, Russia, 1989

Major: Applied Mathematics

Presentations and Publications:

Z.H. Michalopoulou, H. Martynov, and M.B. Porter, "Simulated annealing and genetic algorithms for broadband source focalization," in *Proceedings of the 3rd European Conference on Underwater Acoustics*, edited by J. S. Papadakis, FORTH-IACM, pp.409-414, 1996.

S. Belikov, H. Martynov, and M. Kaplinsky, "Using Wavelength-Dependent Emissivity of Semiconductor Wafer to Model Heat Transfer in Rapid Thermal Processing Station," IEEE Transactions on Semiconductor Manufacturing, **8**, 1995.

S. Belikov, H. Martynov, and M. Kaplinsky, "Design of Rapid Thermal Processing System Based on MSC/NASTRAN Thermal Analysis," in *Proceedings of 1995 MSC World Users Conference*, Universal City, CA, 1995.

S. Belikov, H. Martynov, M. Kaplinsky, C. Manikopoulos, N. Ravindra, and W. Kosonocky, "A Design Methodology for Configuration of Lamps in an RTP System," in *Proceedings of 2nd International Rapid Thermal Processing Conference RTP'94*, Monterey, CA, 1994.

ACKNOWLEDGMENT

This dissertation is dedicated to my yet to be born son, who has already encouraged me to complete this work.

Special thanks go to my husband and NJIT alumni Michael Kaplinsky, whose dedication to his career emphasized the importance of concentrating on one for myself.

The author wishes to express her gratitude to her dissertation advisor Dr. Gregory Kriegsmann for his valuable ideas and contributions to this thesis, as well as for his financial support.

The author also would like to acknowledge Dr. David Stickler, Dr.Jonathan Luke, Dr. Peter Petropoulos, and Dr. Edip Niver for serving as members of the committee.

The author thanks NJIT alumni Dr. Stuart Walker for his friendship and valuable help during the term of this research.

Finally, the author would like to express her appreciation to Roseanne Rowan who assisted me in finding my way from West Coast to Dr. Kriegsmann's office numerous times.

TABLE OF CONTENTS

TABLE OF CONTENTS
(Continued)

LIST OF TABLES

Table **Page**

LIST OF FIGURES

Figure **Page**

LIST OF FIGURES
(Continued)

Figure **Page**

CHAPTER 1

INTRODUCTION

1.1 Problem Statement

Computation of the fields resulting from scattering in waveguides remains one of the most important and challenging problems in wave propagation studies. The complexity of the scattered field depends on the geometry of the problem. Exact formulas for solutions exist only for the geometries admitting separation of variables.

In this dissertation, we develop the approximate solutions for the scattered fields in two practically important geometries: scattering from an object placed inside a stratified waveguide and scattering inside the waveguide with multiple abrupt width transitions.

Although simplified, the first geometry is reasonable for modeling of wave propagation and scattering in many ocean acoustics scenarios. The modeled scattered field can then be further used for localization or shape reconstruction of underwater objects of interest. The second geometry is representative of many practical problems in antenna theory, microwave application and coastal engineering.

Since analytical expressions for the exact solutions are not available for both of the above geometries, the scattered field has to be obtained by numerical methods. Due to the multiple scattering between the waveguide and the object, the solution for the scattered field in the stratified waveguide presents considerable difficulties and is computationally intensive. Similarly, the problem involving our second geometry is also computationally challenging due to scattering from multiple width transitions. However, for certain ratios of characteristic sizes, the solutions for both geometries can be simplified by employing the asymptotic techniques.

In this dissertation, we employ the technique of approximation of the field in the waveguide around the features of small characteristic sizes by the field around the same features in the free space. In the case of the small object inside the stratified

waveguide, the field on the object surface can be approximated by the field on the surface of the same object in the free space. This approximation greatly reduces the computational complexity of the problem as the reflected and transmitted fields now depend on the far field pattern that can be obtained directly from the the shape of the object. Furthermore, the well developed methods for inverse problem in the free space can be extended and adapted to obtain a solution in the waveguide from the scattered field determined by the above approximation. In the case of the waveguide with abrupt width transitions, the scattered field inside the width transition aperture between two waveguide sections can be approximated by the field in the aperture of the waveguide opening into the free space, provided that the width transition is sufficiently large. In this dissertation, we apply the above approximation ideas to our selected geometries and study the resulting accuracy of the solution and the conditions necessary for the approximations to be valid.

1.2 Dissertation Overview

We start every chapter with the review of the relevant existing solutions techniques described in the literature.

In Chapter 2, we consider a direct scattering problem that is realistic for the ocean acoustic environment. The solution for the scattered field is represented as a sum of normal modes obtained by the WKB method. For the case of slowly varying sound speed, we approximate the field on the body within the waveguide by the field on the same body in the free space. We then proceed to investigate the conditions under which this approximation is asymptotically valid. We also demonstrate a technique for modifying our approximation to extend its validity to geometries with obstacles located close to the waveguide boundaries. We present the numerical comparison of the fields on the body within the waveguide and in the free space to confirm the predicted conditions of asymptotic validity.

In Chapter 3, we address the inverse problem of localization and shape reconstruction for the object inside the stratified waveguide. The scattered field approximation developed in Chapter 2 is used for the solution of the direct problem. To simplify the problem of localization of arbitrary shaped target, we employ low frequency methods. We also demonstrate a frequency-independent technique for localization of certain symmetrical targets.

We then proceed to develop the solution for the problem of shape reconstruction of the target placed inside the waveguide. Due to the complexity of this problem, we limit our consideration to high frequency techniques. We adapt techniques well-developed for free space to shape reconstruction of a body inside the waveguide. We also demonstrate the application of the developed inverse techniques by localizing and reconstructing the shape of the circular object from the simulated scattered field data.

In Chapter 4, we consider the scattering of the incident plane wave inside the waveguide with multiple abrupt width transitions. We start by subdividing the complex geometry of the problem into simpler geometrical structures and determine the solutions for the scattered field for each substructure by mode matching technique or by Galerkin method. We then apply the S-matrix method to combine the obtained results in order to describe the field inside the entire structure.

We consider both Dirichlet and Neumann boundary conditions that correspond to electromagnetic and coastal engineering applications. The numerical results for both examples, as well as for electromagnetic receiver and transmitter are presented. Based on numerical results we also conduct the investigation of resonant cavity dimensions.

In Chapter 5, we consider scattering in a waveguide with large abrupt transitions. After non-dimensionalization, the presence of large parameter allows the use of an asymptotic approach to the problem. In this case we employ the

approximation of the field inside the transition region between narrow and wide waveguide by the field inside the aperture of the flanged waveguide. This approximation considerably simplifies the evaluation of the scattering matrix, reducing the numerical complexity of the solution. We then proceed to investigate the conditions necessary for the approximation to be asymptotically valid.

In addition to the asymptotic analysis of the similarity between the actual fields and their approximations, we also present the numerical simulations confirming our theoretical predictions. We then conclude this Chapter by a numerical study of the scattered field obtained by our approximation method. The resonant cavity dimensions are discussed. Finally, the research directions suggested for future work are outlined in Chapter 6.

The Appendix to the dissertation contains the method of matched asymptotics that we developed for acoustic applications. This method is applied to determine the field scattered from the relatively small object submerged inside waveguide. The case of Pekeris waveguide is also considered. We show that the leading order of the resulting expression for the scattered field is equal to the expression obtained in Chapter 2. The method of matched asymptotics confirms the validity of the approximation made in Chapter 2 and can be used if additional accuracy is desired.

CHAPTER 2

DIRECT SCATTERING PROBLEM IN A WAVEGUIDE

2.1 Introduction

Solving a scattering problem in a waveguide presents considerable difficulties, due to the fact that the field produced by the presence of an object is coupled with the field scattered from the waveguide boundaries. Multiple scattering between the object and the boundaries of the waveguide complicates the problem even further. The exact solution, even for the simple shapes of the submerged object, is numerically intensive. Therefore, it is desirable to find a good balance between the efficiency of a model and the full account of the scattering effects.

Several models have been developed to treat the problem for range-independent waveguide [1, 2]. However, the simplification of the problem through the use of asymptotic techniques has not been considered often. The numerical scheme for the small-angle limit in the parabolic equation method [3] is more efficient than non-asymptotic methods but lacks the results for scattered field in the closed form. Another numerical technique, based on Huygens' principle [4], allows the free space solution to be coupled with the solution for a waveguide by matched asymptotics in the intermediate region. The matched asymptotics method presented in Appendix can also be implemented to couple the inner and outer asymptotic expansions of the scattered field. The resulting solution is expressed in terms of the normal modes with the amplitude as a function of the far-field pattern, requiring very few numerical calculations. When more accuracy is desired, the higher terms in asymptotic series can be included in the solution.

Another approach to the scattering problem is based on the assumption that the multiple scattering is negligible, as proposed by Ingenito [5]. This assumption allows him to approximate the scattered field on the surface of the spherical body in a waveguide by the scattered field on the surface of the body in the free space.

Using this approach, the reflection and transmission coefficients for the propagating modes can be easily obtained in terms of the far-field amplitude evaluated at the modal angles. The accuracy of this approximation is not addressed by Ingenito. If the approximation proposed by Ingenito is applied to the field on the body of an arbitrary shape, then it relates the reflection and transmission coefficients that can be measured by an array of receivers to the far field amplitude of the scatterer in the unbounded space. The knowledge of this amplitude allows us to determine the shape of the body by a great variety of methods avoiding the complications of the inversion of the guided far-field operator.

In this Chapter, we study the scattering problem in an ocean with many propagating modes. For these conditions, the numerical evaluation of the exact solution to the integral equation is not feasible, since computations intensify with each propagating mode. We apply asymptotic techniques to derive the expression for the scattered field from submerged object in a horizontally stratified medium with slowly varying sound speed. The characteristic size of the object is taken to be small compared to the depth of the waveguide. Under this assumption, which is met in the ocean acoustic environments, we propose an asymptotic method allowing the solution of the scattering problem for slowly varying sound speed. Furthermore, we propose to validate the approximation made by Ingenito for isovelocity fluid. To estimate the difference between the fields in free space and in the waveguide, we represent it as a solution to an integral equation and obtain a bound on this solution.

2.2 Formulation of the Direct Problem

Let u^i and u^s be the incident and scattered waves, respectively. For a given u^i, we seek the solution to the following problem:

$$\nabla^2 u + (k'n'(z'))^2 u = 0 \qquad \text{in } D/\Omega \tag{2.1}$$

where $D = \{(x', z') : x' \in \mathbf{R},\ 0 \leq z' \leq H\}$; $u = u^i + u^s$;

Ω is convex region, embedded in D, with characteristic length L, $L \ll H$, and centered at (x'_0, z'_0);

with given boundary conditions:

$$\begin{aligned} u &= 0, \quad z' = 0 \\ u_z &= 0, \quad z' = H \\ \frac{\partial u}{\partial \nu} &= 0, \quad \text{on} \quad \partial\Omega \\ & u^s \quad \text{outgoing.} \end{aligned} \tag{2.2}$$

The coordinate system and geometry are illustrated in Fig. 2.1.

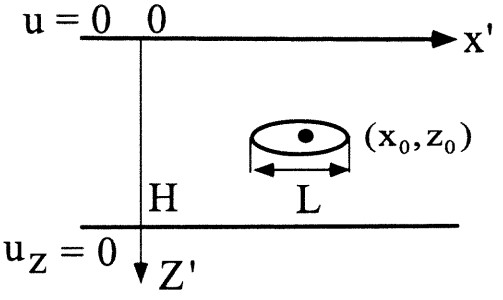

Figure 2.1 Coordinate system and geometry

The scattered field away from the body can be expressed in terms of normal mode representation with unknown reflection and transmission coefficients.

We scale the spatial variables with respect to the depth of the ocean H. In this scaling, the presence of the target is equivalent to the non-isotropic line source in the waveguide of the unit height. The solution for the scattered wave is now expressed in terms of dimensionless variables as

$$u^s = \begin{cases} \sum_{n=0}^{\infty} R_n \Psi_n(\hat{z}) \exp(-ika_n(\hat{x} - \hat{x_0})) & \text{if } \hat{x} < \hat{x_0} \\ \sum_{n=0}^{\infty} T_n \Psi_n(\hat{z}) \exp(ika_n(\hat{x} - \hat{x_0})) & \text{if } \hat{x} > \hat{x_0} \end{cases} \tag{2.3}$$

where $(\hat{x_0}, \hat{z_0})$ is the location of the object, and Ψ_n and a_n are the eigenfunction and the eigenvalue of regular Sturm–Liouville problem.

$$\Psi_n''(\hat{z}) + \hat{k}^2(n(\hat{z})^2 - a_n^2)\Psi_n = 0 \tag{2.4}$$

$$u = 0, \qquad \hat{z} = 0$$

$$u_z = 0, \qquad \hat{z} = 1$$

Assuming $n(\hat{z})$ is monotone, the solution for large values of $\hat{k} = Hk'$ is obtained by WKB method [8] as

$$\Psi_n(\hat{z}) = (n(\hat{z})^2 - a_n^2)^{-1/4} \cos\left(\hat{k} \int_{\hat{z}}^{z_T} \sqrt{n^2 - a_n^2} ds - \frac{\pi}{4}\right), \qquad a_n < n(\hat{z}) \tag{2.5}$$

$$\Psi_n(\hat{z}) = (a_n^2 - n(\hat{z})^2)^{-1/4} \exp\left(-\hat{k} \int_{z_T}^{\hat{z}} \sqrt{a_n^2 - n^2} ds - i\frac{\pi}{4}\right), \qquad a_n > n(\hat{z}) \tag{2.6}$$

where z_T is the turning point and $a_n = n(z_T)$.

2.2.1 Representation of the Reflection and Transmission Coefficients

The unknown reflection and transmission coefficients in Eq. (2.3) carry the information about the shape of the scatterer. To determine these coefficients we set up an integral equation for the total field in the waveguide as

$$\frac{1}{2}u = u_{inc} + \oint_{\partial\Omega} u \frac{\partial G}{\partial \nu} ds \tag{2.7}$$

The scattered field is given by

$$u^s = \oint_{\partial\Omega} u \frac{\partial G}{\partial \nu} ds \tag{2.8}$$

where G is the Green's function for the waveguide given as

$$G(\hat{x}, \hat{z}, \zeta, \eta) = \sum_{n=0}^{\infty} \frac{1}{2ika_n} \Psi_n(\hat{z}) \Psi_n(\eta) \exp(ika_n|\hat{x} - \zeta|) \tag{2.9}$$

Since the size of the scatterer is small, $L/H \ll 1$, we look for the asymptotic approximation of the Green's function on the boundary of the scatterer, that is described by $\hat{z} = \hat{z_0} + \bar{z}, \hat{x} = \hat{x_0} + \bar{x}$, where $\bar{z}$ and $\bar{x}$ describe the surface of the scatterer and have the order of $\frac{L}{H}$. Assuming that the sound speed is slowly varying

function of depth and the turning point z_T is away from z_0, the Green's function can be approximated as

$$G(\hat{x},\hat{z},\zeta,\eta) \sim \sum_{n=0}^{\infty} \frac{1}{4ika_n\sqrt{k_n}} \Psi_n(\eta) \exp(ika_n|\hat{x}-\zeta|)(e^{ikq_n - i\frac{\pi}{4}} e^{-ikk_n\bar{z}} + e^{-ikq_n + i\frac{\pi}{4}} e^{ikk_n\bar{z}}) \tag{2.10}$$

where $q_n = \int_{z_0}^{z_T} \sqrt{n(s)^2 - a_n^2}\, ds$, and $k_n^2 = n^2(z_0) - a_n^2$.

Differentiation of the above expression and the substitution of the resulting expression into the equation (2.8) leads to the values of the reflection and transmission coefficients

$$\begin{aligned} R_n &= \frac{1}{4ika_n\sqrt{k_n}}[e^{-ikq_n+i\frac{\pi}{4}} \oint_{\partial\Omega} u(n_x a_n + n_z k_n) e^{ik(k_n\bar{x}+a_n\bar{z})} ds \\ &+ e^{ikq_n - i\frac{\pi}{4}} \oint_{\partial\Omega} u(n_x a_n - n_z k_n) e^{ik(k_n\bar{x}-a_n\bar{z})} ds] \qquad (2.11) \\ T_n &= \frac{1}{4ika_n\sqrt{k_n}}[-e^{-ikq_n+i\frac{\pi}{4}} \oint_{\partial\Omega} u(n_x a_n + n_z k_n) e^{ik(-k_n\bar{x}+a_n\bar{z})} ds \\ &+ e^{ikq_n - i\frac{\pi}{4}} \oint_{\partial\Omega} u(-n_x a_n + n_z k_n) e^{-ik(k_n\bar{x}+a_n\bar{z})} ds] \qquad (2.12) \end{aligned}$$

The approximation of the field on the body in the waveguide (or its normal derivative for sound hard bodies) by the field on the body in free space, suggested by Ingenito [5], let us to determine the coefficients as functions of the far-field pattern in free space:

$$T_n = \frac{1}{4ika_n\sqrt{k_n}}[e^{-ikq_n+i\frac{\pi}{4}} \cdot A(-\theta_n) + e^{ikq_n - i\frac{\pi}{4}} \cdot A(\theta_n)] \tag{2.13}$$

$$R_n = \frac{1}{4ika_n\sqrt{k_n}}[e^{-ikq_n+i\frac{\pi}{4}} \cdot A(\pi+\theta_n) + e^{ikq_n - i\frac{\pi}{4}} \cdot A(\pi-\theta_n)] \tag{2.14}$$

where

$$A(\theta) = \oint_{\partial\Omega} u_{freespace}(\hat{n}\cdot\hat{r}(\theta)) e^{-ik\vec{x}\cdot\hat{r}(\theta)} ds \tag{2.15}$$

is the far field pattern with spatial variables scaled by the characteristic size of the target, and $\theta_n = \arctan\frac{k_n}{a_n}$ is the eigen-angle of the n-th mode.

The incident wave is taken to be a single propagating mode which can be decomposed into two plane waves. The superposition principle is used to formulate

the expression for the scattered field in the presence of a line source that excites N propagating modes.

The method of matched asymptotics outlined in the Appendix results in the expression for the reflection and transmission coefficients that in its leading order is equal to the expression given by Eqs. (2.13)-(2.14).That confirms that the approximation applied above is valid under conditions assumed by the method of matched asymptotics.

We can extend the obtained results to the case of the scatterer located close to one of the boundaries. The approximation of the total field on the body in the waveguide by the field on the body in half space can be determined as a solution to the integral equation $u_{h.s.} = u_{inc} + \oint u_{h.s.} \frac{\partial \Phi}{\partial \nu} ds$. The Green's function, Φ, for half space is found by image method and depends on the given condition for the field on the half space boundary. The reflection and transmission coefficients are still described by Eqs. (2.14)-(2.13), where $A(\theta)$ is now the far-field amplitude for the half space field given by $A(\theta) = \oint_{\partial\Omega} u_{h.s.}(\hat{n} \cdot \hat{r}(\theta)) e^{-i\bar{k}\vec{x}\cdot\hat{r}(\theta)} ds$.

2.3 Approximation of the Field on the Body of the Scatterer

In this section, we determine an asymptotic estimate of the upper bound for the difference between the scattered fields on the body. Let ϑ be the total field in the free space, u be the field in the waveguide, and $\triangle$ is the difference, i.e.

$$\triangle = \vartheta - u \tag{2.16}$$

The scatterer is assumed to be small compared to the depth of the waveguide, i.e. $y = \frac{H}{L} \gg 1$. The spatial variables are scaled by the size of the object, $x = \frac{x' - x'_0}{L}$ and $z = \frac{z' - z'_0}{L}$, $k = k'L$. Therefore, the depth of the waveguide is y. The object is located at $(0, 0)$, the waveguide boundaries are located at $z = -\frac{y}{a}$ and $z = y - \frac{y}{a}$,

and $a = \frac{H}{z_0'}$ represents the location of the object inside the waveguide in relation to the depth of the waveguide.

The difference $\triangle$ is the solution to the integral equation

$$\frac{1}{2}\triangle = h + \oint_{\partial\Omega} \triangle \frac{\partial G_{w.g.}}{\partial \nu} ds \tag{2.17}$$

where $G_{w.g.}$ is the Green's function for the waveguide, $H_{f.s.}$ is the free space Green's function, and the forcing term h is given by

$$h = \oint_{\partial\Omega} \vartheta \frac{\partial (G_{w.g.} - H_{f.s.})}{\partial \nu} ds \tag{2.18}$$

Therefore, the bound on $\triangle$ is controlled by h, which is described by the difference between the normal derivatives of the Green's functions on the body in the waveguide and in free space.

Near the body the index of refraction, $n(z_0 + \frac{z}{y})$, can be approximated by a constant $n_0 = n(z_0)$, provided that the sound speed in the waveguide is slowly varying. Since we are looking for the solution of the integral equation (2.17) on the body, we can limit ourselves to the case of a homogeneous medium.

The free space Green's function for the free space in homogeneous medium, $n = n_0$, is given by

$$H = -\frac{i}{4} H_0^{(1)}(k n_0 \rho) \tag{2.19}$$

where $\rho^2 = (x - \xi)^2 + (z - \eta)^2$.

The Green's function for the waveguide is determined by the image method for given boundary conditions as

$$G = \frac{i}{4} \sum_{l=-\infty}^{\infty} (-1)^l [H_0^{(1)}(k n_0 \rho_l) - H_0^{(1)}(k n_0 \hat{\rho}_l)] \tag{2.20}$$

where

$$\begin{aligned} \rho_l^2 &= (x - \xi)^2 + (z - \eta_l)^2, \\ \eta_l &= \eta + 2ly \end{aligned}$$

$$\begin{aligned}\hat{\rho}_l^2 &= (x-\xi)^2+(z-\hat{\eta}_l)^2,\\ \hat{\eta}_l &= -\eta+2ly-\frac{2y}{a}\end{aligned}$$

The difference between the normal derivatives of H and G is given by

$$\begin{aligned}\frac{\partial}{\partial\nu}(H-G) &= -\frac{i}{4}kn_0[H_1^{(1)}(kn_0\hat{\rho}_{l=0})\\ &- \sum_{l\neq 0}(-1)^l(H_1^{(1)}(kn_0\rho_l)-H_1^{(1)}(kn_0\hat{\rho}_l))]\frac{d\rho}{d\nu}\end{aligned} \tag{2.21}$$

If the body is positioned far away from the boundaries of the waveguide, i.e. $a=1+b$ for $b=O(1)$, then the distances ρ_l and $\hat{\rho}_l$ can be approximated as

$$\begin{aligned}\rho_l &\approx 2y|l|,\\ \hat{\rho}_l &\approx 2y(l-\frac{1}{a}), \quad l>0\\ \hat{\rho}_l &\approx 2y(|l+\frac{1}{a}|), \quad l\leq 0,\end{aligned} \tag{2.22}$$

respectively.

If we further assume that the wavelength is much smaller than the width of the waveguide, i.e. $k'n_0D=kn_0y\gg 1$, then the difference given by Eq. (2.21) can be expressed asymptotically as

$$\begin{aligned}\frac{\partial}{\partial\nu}(H-G) &\sim -\frac{1}{4}\sqrt{\frac{kn_0a}{\pi y}}e^{i(\frac{2kn_0y}{a}-\frac{3\pi}{4})}+\frac{1}{4}\sqrt{\frac{kn_0}{\pi y}}e^{-i\frac{3\pi}{4}}\sum_{m=1}^{\infty}(-1)^m[\frac{2}{\sqrt{m}}e^{2ikn_0my}\\ &- \frac{\sqrt{a}}{\sqrt{am-1}}e^{2ikn_0\frac{am-1}{a}y}-\frac{\sqrt{a}}{\sqrt{am+1}}e^{2ikn_0\frac{am+1}{a}y}]\end{aligned} \tag{2.23}$$

Therefore,

$$|\frac{\partial}{\partial\nu}(H-G)|\leq\frac{1}{4}\sqrt{\frac{kn_0a}{\pi y}}+\frac{1}{4}\sqrt{\frac{kn_0}{\pi y}}|\sum_{m=1}^{\infty}e^{iv m}(\frac{2}{\sqrt{m}}-\frac{\sqrt{a}e^{-i\frac{v}{a}}}{\sqrt{am-1}}-\frac{\sqrt{a}e^{i\frac{v}{a}}}{\sqrt{am+1}})| \tag{2.24}$$

where $v=2kn_0y+\pi$

We represent the series in Eq.(2.24) as a sum of two pieces, S_1 and S_2:

$$S_1=i\sqrt{a}\sin\frac{v}{a}\sum_{m=1}^{\infty}e^{imv}(\frac{1}{\sqrt{am-1}}-\frac{1}{\sqrt{am+1}}) \tag{2.25}$$

$$S_2 = \sum_{m=1}^{\infty} e^{imv}\left(\frac{2}{\sqrt{m}} - \frac{\sqrt{a}\cos\frac{v}{a}}{\sqrt{am-1}} - \frac{\sqrt{a}\cos\frac{v}{a}}{\sqrt{am+1}}\right) \tag{2.26}$$

First, we consider the series S_1, which is absolutely convergent and bounded. The bound is obtained by the integral test as

$$|S_1| \le |\sin\frac{v}{a}|\left(\sqrt{1+\frac{1}{a}} - \sqrt{1-\frac{1}{a}}\right) \tag{2.27}$$

To bound the second series S_2 we represent it as a sum of three parts

$$\begin{aligned} S_2 = 2\sin^2\frac{v}{2a}\sum_{m=1}^{\infty}\frac{e^{imv}}{\sqrt{m}} &+ \cos\frac{v}{a}\sum_{m=1}^{\infty} e^{imv}\left(\frac{1}{\sqrt{m}} - \frac{\sqrt{a}}{\sqrt{am-1}}\right) \\ &+ \cos\frac{v}{a}\sum_{m=1}^{\infty} e^{imv}\left(\frac{1}{\sqrt{m}} - \frac{\sqrt{a}}{\sqrt{am+1}}\right) \end{aligned} \tag{2.28}$$

Then

$$\begin{aligned} |S_2| \le 2\sin^2\frac{v}{2a}\left|\sum_{m=1}^{\infty}\frac{e^{imv}}{\sqrt{m}}\right| &+ \sqrt{a}\left|\cos\frac{v}{a}\right|\left(\sum_{m=1}^{\infty}\left|\frac{1}{\sqrt{m}} - \frac{\sqrt{a}}{\sqrt{am-1}}\right|\right. \\ &+ \left.\sum_{m=1}^{\infty}\left|\frac{1}{\sqrt{m}} - \frac{\sqrt{a}}{\sqrt{am+1}}\right|\right) \end{aligned} \tag{2.29}$$

The series $\sum\frac{e^{imv}}{\sqrt{m}}$ are the divergent series for $v = 2n\pi$. For these values of v the wavenumber k is an eigenvalue for the waveguide problem, and the Green's function G does not exist. This case excluded, the series are convergent for any other value of v by the Dirichlet's test, since $\{|\sum_{m=1}^{n} e^{imv}|\}$ is a bounded sequence, and $\{m^{-\frac{1}{2}}\}$ is a decreasing sequence convergent to 0. Moreover, $\sum\frac{e^{imv}}{\sqrt{m}} = \frac{1}{\sqrt{\tilde{v}}}e^{i\frac{\pi}{4}} + O(1)$ by Poisson summation formula [7], where $\tilde{v} = v - 2n\pi \in (0, 2\pi)$.

The series $\sum|\frac{1}{\sqrt{m}} - \frac{\sqrt{a}}{\sqrt{am-1}}|$ are convergent by the integral test, and bounded by $\frac{1}{\sqrt{a}}(1-\sqrt{1-\frac{1}{a}})$. The same reasoning applies to the last series in Eq. (2.29).

Therefore, the bound on the series S_2 is determined as

$$|S_2| \le 2\sin^2\frac{v}{2a}\left(\frac{1}{\sqrt{\tilde{v}}} + O(1)\right) + |\cos\frac{v}{a}|\left(\sqrt{1+\frac{1}{a}} - \sqrt{1-\frac{1}{a}}\right) \tag{2.30}$$

Substitution of the results given in Eqs. (2.27)-(2.30) into Eq. (2.24) produces the asymptotic bound for the difference (2.21) as

$$|\frac{\partial}{\partial\nu}(H-G)| \le \frac{1}{4}\sqrt{\frac{kn_0}{\pi y}}[\sqrt{a} + |S_1| + |S_2|] = O\left(\sqrt{\frac{kn_0}{\pi y}}\right) \tag{2.31}$$

Therefore, the forcing term h, given by Eq. (2.18), is of order $\sqrt{\frac{kn_0}{y}} \ll 1$. The difference $\triangle$, given by Eq. (2.17), is equivalent to the total field in the waveguide produced by the wave h incident on the target. Therefore, in the absence of resonance, $\triangle$ has at most the same asymptotic order as h, i.e. $\triangle = O(\sqrt{\frac{kn_0}{y}})$.

To show that the solution to the Eq. (2.17) exists and that it is close to zero under the above conditions, we represent the Eq. (2.17) using the operator notation as

$$(I + 2H + 2D)\triangle = 2h \tag{2.32}$$

where

$$\begin{aligned} H(u) &= \frac{i}{4}\oint H_0^{(1)}(k\rho)uds \\ D(u) &= \sum_{n\neq 0}(-1)^n[\oint H_0^{(1)}(k\rho_n)uds + \oint H_0^{(1)}(k\hat{\rho}_n)uds \end{aligned} \tag{2.33}$$

Since ϖ is the free space solution of the equation $(I + 2H)\varpi = 2u^{inc}$, the operator $(I + 2H)^{-1}$ exists when $(kn_0)^2$ is not an eigenvalue of the adjoint interior problem [9]. Therefore, the operator $(I + 2H)^{-1}$ is bounded and its' norm is less than a constant $M = O(1)$. Under the same hypothesis on $(kn_0)^2$, the Eq. (2.32) has the solution $\triangle = 2(I + 2H + 2D)^{-1}h$ if the operator $(I + \frac{2D}{I+2H})^{-1}$ is bounded.

For the given assumptions, $y \gg 1$, $ky \gg 1$, and $a = 1 + O(1)$, we find the estimate on the norm of D as

$$\|D\| \sim \frac{1}{2\|u\|}[\frac{\sqrt{a}}{\sqrt{y}}\oint \exp(ik\frac{y}{a})uds + \frac{C}{\sqrt{y}}\oint \exp(iky)uds] = O(\frac{1}{y}) \tag{2.34}$$

From this estimate, we can conclude that $\|D\| < \frac{M}{2}$ and $\|\frac{2D}{I+2H}\| < 1$. Then the operator $(I + \frac{2D}{I+2H})^{-1}$ can be represented by Neumann series as

$$(I + \frac{2D}{I+2H})^{-1} = I - \frac{2D}{I+2H} + ... \sim I + J \tag{2.35}$$

where $\|J\| = O(\frac{1}{y})$.

The difference between the fields on the body in free space and in the waveguide is approximated by

$$\triangle = 2(I+2H)^{-1}(I+\frac{2D}{I+2H})^{-1}h \sim 2(I+2H)^{-1}h = O(\sqrt{\frac{kn_0}{y}}) \qquad (2.36)$$

.

2.3.1 Multiple Scattering Effects

As was mentioned earlier, in order to include the effects of multiple scattering for the target located close to one of the boundaries, the field on the body in the waveguide is approximated by the field on the body in a half space. To analyze this approximation, we use the same approach as above.

If the object is close to the upper boundary, i.e. $a \sim y$, then in Eq.(2.22) $\rho_m \sim O(1)$ for $m = 0$, multiple scattering between the target and the upper boundary is no longer negligible. However, the difference between the normal derivatives of the Green's function for the half space and the Green's function for the waveguide is now determined as

$$\begin{aligned} \frac{\partial}{\partial \nu} \quad & (H_{h.s.} - G) \sim \frac{1}{4}\sqrt{\frac{kn_0}{\pi y}}(|S_1| + |S_2|) \\ \leq \quad & \frac{1}{2a}\sqrt{\frac{kn_0}{\pi y}}(\sin\frac{v}{a} + \cos\frac{v}{a} + a\sin^2\frac{v}{2a}(\frac{1}{\sqrt{\tilde{v}}} + O(1))) = O(\sqrt{\frac{kn_0}{\pi y}}) \end{aligned} \qquad (2.37)$$

Therefore, the approximation of the field on the body of the scatterer in the waveguide by the field on the body in the half space takes into account multiple scattering from the closely located upper boundary. We may note that for the certain values of the wavenumber $ky \approx (2an-1)\frac{\pi}{2}$ we can expect the approximation to be much more accurate than the approximation for the body located in the middle of the waveguide, since for these values of ky the difference in Eq. (2.37) has the order of $y^{-\frac{3}{2}}$

If the object is located near the lower sound hard boundary, i.e. $a \sim 1 + O(\frac{1}{y})$, then the difference between the normal derivatives of the Green's function for the

half space and the Green's function for the waveguide is estimated as

$$\frac{\partial}{\partial \nu}(H_{h.s.} - G) \sim \frac{1}{4}\sqrt{\frac{kn_0}{\pi y}}(\sqrt{a} + \sqrt{2}\cos\frac{\upsilon}{a} + \sin\frac{\upsilon}{a} + 2\sin^2\frac{\upsilon}{2a}(\frac{1}{\sqrt{\upsilon}} + O(1)) = O(\sqrt{\frac{kn_0}{\pi y}}) \tag{2.38}$$

Therefore, the approximation of the field on the body in the waveguide by the field in the half space has at least the same asymptotic order of accuracy as the approximation for the field on the body located away from the boundaries.

2.4 Numerical Simulations

As the test problem, we modeled the scattering from the circular sound hard object with radius 1. The exact solution for the total field on the body in free space is well known, and given as

$$\vartheta = \frac{2}{\pi k}\sum_{n=0}^{\infty}\varepsilon_n\frac{(-i)^{n-1}}{H_n^{'(1)}(k)}\cos n(\theta - \beta) \tag{2.39}$$

The incident field is a plane wave traveling in the direction $\pi - \beta$, i.e. $u^i = e^{-ikr\cos(\Phi-\beta)}$.

The total field in the waveguide is obtained as a solution of the integral equation

$$u_{wg}(\Phi) = u^i + 2\int_{-\pi}^{\pi} u(\theta)\frac{\partial G_{w.g.}}{\partial \nu}d\theta \tag{2.40}$$

where $G_{w.g.}$ is given by Eq. (2.20). The series in Eq. (2.20) is truncated when $G_{w.g.}$ is accurate up to 10^{-4}. This integral equation is solved by Nystrom method with 40-point Gauss-Chebyshev quadrature. The resulting linear system is then solved by Gauss elimination.

The comparison of the calculated total fields on the body in the waveguide with the total field in free space is shown in Figures 2.2- 2.4. The scattered field is exited by the 50-th incident mode of the amplitude 1 and the directional angle $\beta = \arcsin(\frac{50.5\pi}{220})$.

First, we research the variation in the amplitude and the phase of the total on the body resulting from the change in the waveguide depth. We position the target

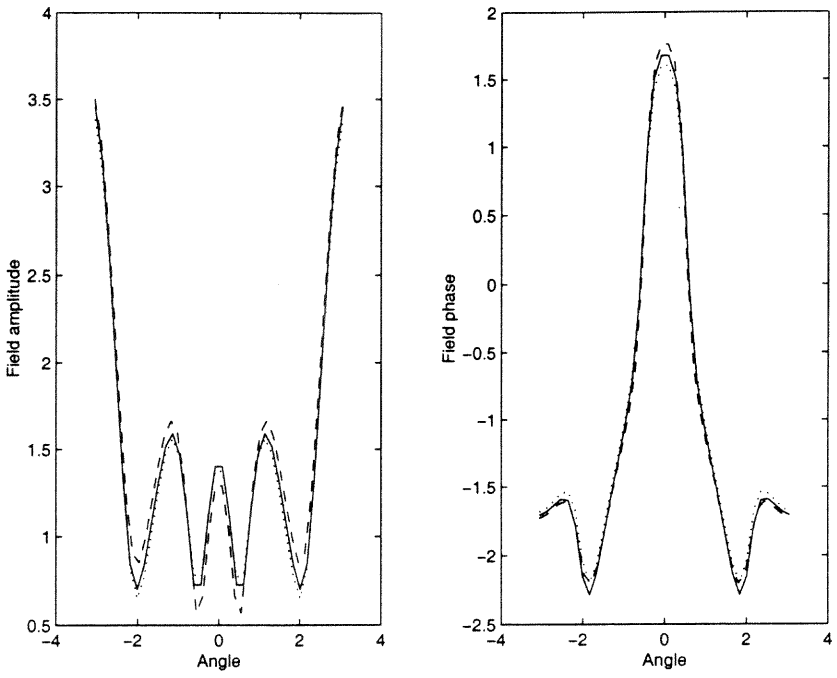

Figure 2.2 Total field for k=2.2. Exact field in free space is shown by the solid line; y=50 is shown by the dashed curve; y=100 is shown by the dotted curve.

in the middle of the waveguide, $a = 2$, fix the frequency at $k = 2.2$, and vary the value of the depth y. The comparison with the field in free space is shown in Figure 2.2. We can see that the field in free space is better approximation for the field in the waveguide with bigger value of y. The relative error for the depth $y = 100$ is way below expected 10%.

We investigate the accuracy of the approximation for the variable frequency in Figure 2.3. The depth of the waveguide is fixed at $y = 100$, the body location is given as $a = 2$. We note that the curves for the lower frequencies fit the curve for the field in the free space better. That is expected from the approximation presented in previous section.

In Figure 2.4, we show the total field amplitude for the different locations of the scatterer inside the waveguide. We observe that the multiple scattering effects become more pronounced as the body is moved closer to the boundaries. We may also

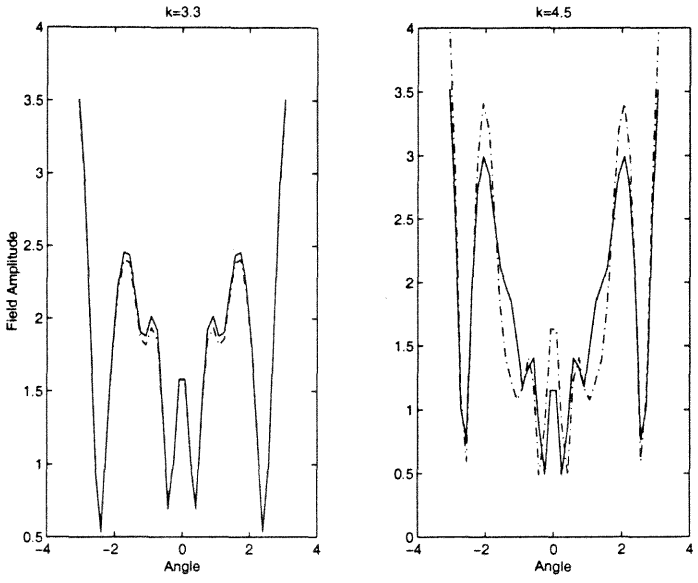

Figure 2.3 Total field in free space (solid line) vs. field in the waveguide (dashed line) for y=100, a=2. (A) k=3.3, (B) k=4.5.

note that the graphs for the field scattered from the target located close to the upper boundary (shown in Fig. 2.4A) are in better agreement with the field in free space, than the graphs for the field scattered from the body located at the same distance from the lower boundary (Fig. 2.4B). This effect is due to the different conditions on the boundaries. The results of the Section 2.3 bound the order of the absolute error for both approximations by $\sqrt{\frac{kn_0}{d}}$. But considering the whole expression for the bound, given by Eqs. (2.31), (2.27)-(2.30), we can predict that the error for the target near the upper boundary is smaller than for the target near the lower boundary, since the bound is given as

$$A \ : \ \frac{1}{4}\sqrt{\frac{kn_0}{y}}(1+2\sin^2\frac{v}{2a}\sqrt{\frac{d}{y}}), \quad \text{upper boundary;}$$

$$\text{vs } B \ : \ \frac{1}{4}\sqrt{\frac{kn_0}{y}}(1+\sqrt{\frac{d}{y-d}}O(1)), \quad \text{lower boundary;}$$

At the same time, the field produced by the scattering from the body located near the boundaries represents close approximation of the field in the half space, as

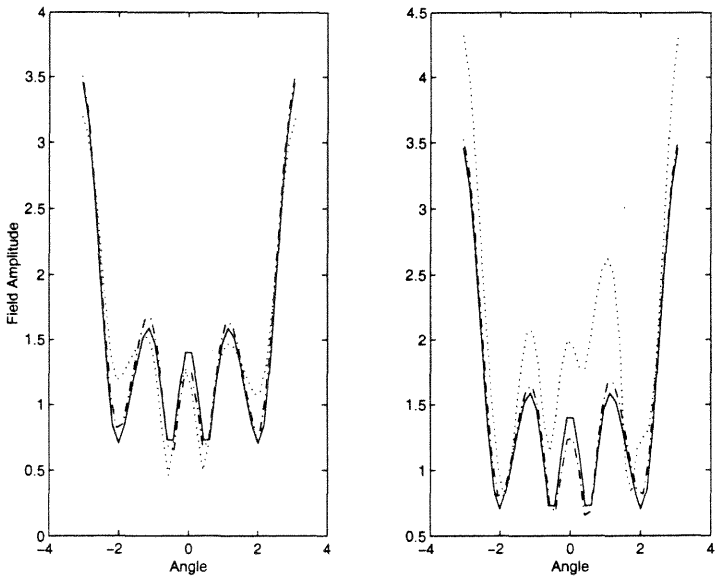

Figure 2.4 Total field for k=2.2, y=100. Field in free space is shown by the solid line.
(a) Object is close to the upper boundary: at distance d=$\frac{100}{6}$ - dashed line, at distance d=2 - dotted line.
(b) Object is at the same distance from the lower boundary.

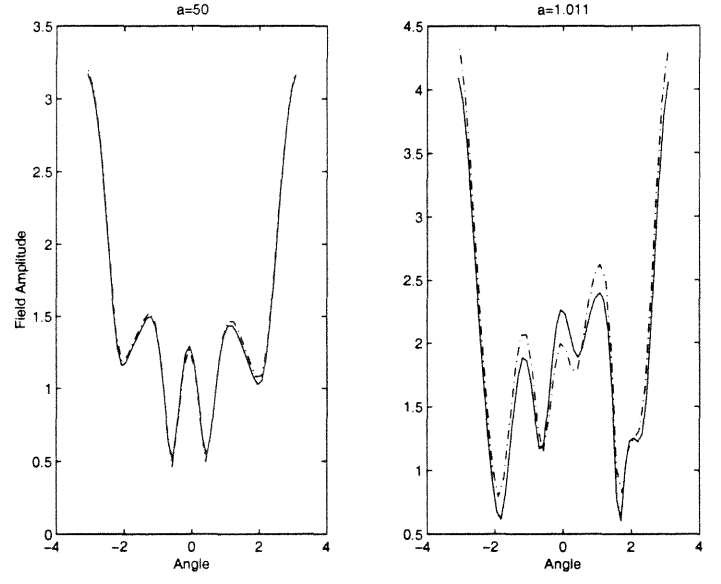

Figure 2.5 Field in the half space(solid line) and field in the waveguide (dashed line).
(a) d=2 from upper boundary: (b) d=2 from lower boundary.

shown in Fig. 2.5. The field in the half space is obtained as a solution of the integral equation (2.7) for the appropriate Green's function found by the image method. As was predicted, better accuracy is achieved when the object is close to the upper boundary.

2.5 Conclusions

The solution for the field scattered from a small body in a range independent waveguide is obtained in terms of the normal modes. The normal modes coefficients are dependent on the location of the scatterer and its shape. It was shown what assumptions on the size of the scatterer, the depth of the waveguide, and the wavenumber are necessary in order for the solution to be asymptotically valid.

The estimate of the accuracy of the approximate scattered field under given assumptions was obtained. It was also shown under what conditions on the location of the body inside the waveguide the multiple scattering effects can be neglected. The adjustments to maintain the desired asymptotic accuracy were implemented when these conditions were not satisfied. The numerical simulations were conducted for the different conditions of the waveguide. The simulated results are shown to be in agreement with the analytical considerations on the validity of the solution for the scattered field and the predicted accuracy of the solution.

CHAPTER 3

INVERSE PROBLEM IN A STRATIFIED WAVEGUIDE

3.1 Introduction

As was shown in the previous Chapter, the reflected and transmitted scattered fields depend on the values of the far field pattern in free space. If we are able to obtain the far field pattern from the measurements of the scattered field, we can then implement any classical inverse method to determine the shape of the target. In the realistic ocean environment, the field is measured by a discrete number of hydrophones, and the modal reflection and transmission coefficients are obtained from these measurements. The recovery of the modal coefficients does not provide enough information to determine the far field pattern, since each coefficient is dependent on the magnitude of the far field pattern at two distinct points as well as the body location. Therefore, the adjustments to the classical inverse methods are necessary to determine the shape of the scatterer.

The inverse problem can be formulated as follows

- Given a vector of measurements of the scattered field on a vertical array of M hydrophones, determine the location and type (or the complete shape, if possible) of the target.

A wide range of array processing methods has been employed for source localization in the ocean acoustics. The arrival pattern of the signal in time domain has been used in modal travel-time and peak arrival methods [10]. The overview of a variety of processors used in frequency domain can be found in [12]. One of the most powerful frequency domain methods is matched field processing. The idea behind this method consists of placing a test point source at different locations of a search grid, computing the field at all elements of the receiver array, and then correlating this simulated field with measured data from the point source of unknown location.

The maximum correlation is obtained when the test and real sources are co-located. Recently the methods of simulated annealing and genetic algorithms were applied to improve efficiency of the maximization process [13, 14].

To implement matched field processing as an inversion scheme for the normal mode representation of the scattered field given by Eq. (2.3), we have to deal with an additional $4N$ unknowns that represent the values of the far field pattern for eigen-angles of N propagating modes. Since we have no a priori knowledge about these values, we would have to conduct the search over a wide range of these parameters. Furthermore, we would have to establish a fine search grid over the entire range of feasible parameter values to determine the values of the far field patterns with required accuracy. Finding maximum correlation between replica and measured fields under these conditions becomes very computationally expensive problem, sensitive to mismatch.

For a given inverse problem, an alternative approach to the use of the matched field processing can be employed. Instead of looking for specific values of the far field pattern that are used in the expression for the replica fields, given by Eqs. (2.14)-(2.13), we can model the replica fields for a variety of assumed shapes and different locations of the body. Once the far field pattern for a certain shape is obtained, it can then be used together with an assumed location of the scatterer to determine each solution to the direct scattering problem. These solutions are matched with the measured field in the processor.

A different processing technique to localize the source, that does not require detailed modeling, has also been investigated by the researchers in ocean acoustics [15, 16]. The method, called mode matching, takes advantage of the fact that the field in a waveguide can be represented in terms of normal modes, and uses modal decomposition followed by range and depth beamforming to obtain matched mode processor.

The localization of the extended target in a waveguide is a more complicated than localization of the point source, since there exists a mode coupling between the incident and the scattered modes. The matched mode processing can not be readily applied to the formulated inverse problem, since the mode coefficients are dependent on the far field pattern of the scatterer in addition to its location. The broadband matched mode processing for active source localization was applied to scattered field by Yang and Yates [17]. This method allows to detect and localize the target when the relative phases of mode arrivals are not distorted by the scattering function of the target.

In Section 3.2, we consider the problem of target localization. We implement mode filtering, proposed in [15], to obtain the reflection and transmission coefficients for the propagating modes in frequency domain. We then use these coefficients in two different processors that we developed for the symmetrical target and for low frequency of the incident field. The results of the numerical simulations are presented for both types of the localization schemes.

Once the target has been localized, the next step in the solution of inverse problem is to determine the type or shape of the target. Extensive research has been conducted on the inverse problem of determining the shape of an obstacle in an unbounded environment. Low frequency methods, such as the Born approximation, and high frequency methods, such as physical or geometrical optics, have been developed to recover either the volume or the shape of an obstacle. The ongoing research of Colton and Kress has addressed the problem of reconstructing the shape of the scatterer from the knowledge of the far field pattern for objects dimensions comparable with the wavelength. The overview of this work can be found in [18],[9].

The problem of determining the shape of an obstacle in a bounded environment, such as a stratified waveguide representing a finite depth ocean is an even more difficult problem. In this case the scattered field propagates in the form of guided

modes. In the far field of the scatterer only the propagating modes can be detected, therefore some information about the shape of the scatterer is inevitably lost.

The identification of a passive body in a shallow water has been an object of considerable research. Different optimization schemes have been employed to match the shape of the scatterer with the far-field pattern of the guided wave [19, 20]. To obtain the far-field pattern of the guided wave, the scattered field has been represented as a solution of the boundary integral equation involving the Green's function for the waveguide. In a similar optimization scheme of nonlinearized complete family methods, the scattered field is determined as a finite sum of Green's functions whose source locations evolve with the obtained contour [22]. Because of the complexity of the direct scattering, these solutions require very intensive computations.

The approximation of the solutions to the direct problem is one of the approaches that can be taken to simplify the inverse problem. The approximation of the scattered field by canonical solutions for a sphere in the free space [23] or a cylinder in a waveguide [24] allows to employ the matching of trial objects and measured fields.

A priori knowledge about the type of the target is another simplification allowing to determine the full information about the target shape. Mode matching techniques, similar to the methods applied in Chapter 4, have been recently employed to determine the dimensions of a cylindrical pillbox [25].

In the inverse scheme proposed in this dissertation, we use the approximation of the direct problem solution obtained in Chapter 2. These approximate solutions for the scattering problem in a waveguide are dependent on the far field solutions for the same object in the free space. Therefore, we will extend the methods for shape retrieval in an unbounded environment and tailor them for the application to the inverse problem in a stratified waveguide.

We limit ourselves to the high frequency inverse methods. In Section 3.3 we present the geometrical and physical optics approach to the reconstruction of the symmetrical and non-symmetrical objects inside the wide stratified waveguide. The numerical results of the optimization procedure proposed for non-symmetrical bodies are then presented and discussed.

3.2 Target Localization

The reflection and transmission coefficients of the scattered field carry the information about the location and the shape of the scatterer To determine these coefficients from the measured field we use mode decomposition technique.

The scattered field is measured by a vertical array of M receivers located at $(0, z_j)$. The value of the acoustic pressure at each hydrophone is represented by the sum of N propagating modes as

$$P(z_j) = \sum_{i=1}^{N} \Psi_i(z_j) a_i \tag{3.1}$$

The values of $\Psi_i(z_j)$ are calculated for each mode and each receiver location, and the resulting linear system $\vec{P} = E\vec{a}$ is solved for $\vec{a}$ by either least square methods (to minimize the noise) or by eigenvector decomposition.

The detailed discussion of the advantages and effectiveness of the various solution techniques for mode decomposition is found in [15]. From now on, we will assume the coefficients a_i to be known, and will refer to them as measured reflection coefficients r_n when the reflected scattered field was measured, or measured transmission coefficients t_n in case of transmission measurements.

The field scattered from the object is produced by the single incident mode. The beamforming procedure of a single low mode generation by an array of sources is described by Sarkissian [27]. In the present work, we consider finite depth waveguide. The solution to the direct problem can be obtained by asymptotic methods as

described in previous chapter and is given by Eq. (2.3) We use this solution as a simulated replica field in the processor. The analytical representation of the reflection and transmission coefficients is given by Eqs. (2.14)-(2.13).

3.2.1 Low Frequency Processor

In the first case under consideration, consistent with the assumptions made in Chapter 2, we assume low frequency propagation, $kn_0 \ll 1$ where k is a wavenumber scaled with respect to the size of the object. Under this assumption the far field pattern can be expanded in the convergent series [28]

$$A(\theta) = \sum_{m=0}^{\infty} A_m(\theta, \beta) k^m. \tag{3.2}$$

For the sound soft scatterer, the leading term in the above expression is a constant independent of the scattering angle. Therefore, the reflection and transmission coefficients for the propagating modes of the scattered field can be approximated as

$$\begin{aligned} R_n &\sim C_n A \Psi_n(z_0) e^{ika_n x_0} \\ T_n &\sim C_n A \Psi_n(z_0) e^{-ika_n x_0} \end{aligned} \tag{3.3}$$

where $C_n = \frac{1}{2ika_n\sqrt{k_n}}$.

The range location of the scatterer can be determined by any time domain localization method, since the scattering away from the body is equivalent to a propagation from a line source. Therefore, the range dependence of the acoustic field is not influenced by the shape of the scatterer.

To obtain the vertical location of the scatterer, we use the beamforming process and construct the depth function as

$$D(z) = |\sum r_n \rho_n \Psi_n(z)| \tag{3.4}$$

where the shading coefficient $\rho_n = \frac{e^{-ika_n x_0}}{C_n}$. Therefore, the highest order of the depth function is given as

$$D(z) \sim |\sum_{n=1}^{N} \Psi_n(z_0)\Psi_n(z)| \sim \delta(z - z_0) \tag{3.5}$$

Since the peak of the depth function is achieved at $z = z_0$, the maximization of the depth function yields the vertical coordinate of the scatterer location.

If the range location of the target is unknown but the measurements for both reflected and transmitted fields are available, we can still construct the processor to determine the vertical position of the scatterer. The range independent processor is defined as

$$\frac{1}{C_n^2}(r_n t_n - R_n T_n) = \frac{1}{C_n^2}(r_n t_n - A^2\Psi_n^2(z_0) + noise) \tag{3.6}$$

To minimize the absolute value of the processing difference given by Eq. (3.6) over all propagating modes and to obtain the vertical location of the scattering object, we use the method of least squares. Our goal is to solve the following minimization problem:

$$\underbrace{\min}_{A_1,A_2,z_0} \sum_{n=0}^{N} (Re(r_n t_n) - A_1\Psi_n(z_0))^2 + (Im(r_n t_n) - A_2\Psi_n(z_0))^2 \tag{3.7}$$

Though the approximation for the square of the far field pattern is a real number, we still include imaginary part in minimization to compensate for neglected terms in the series expansion. A variety of numerical iteration and gradient methods are applicable to this minimization problem.

If the scatterer is sound hard, the leading order in reflection coefficient can be represented as

$$R_n \sim 2C_n(A + S(\theta_n)S(\beta))\Psi_n(z_0)e^{ika_n x_0} \tag{3.8}$$

where A is the area of the scatterer and S is a trigonometric funtion of the scattering angle θ_n or incident angle β [17].

Under assumptions of Chapter 2, the values of function $S(\theta_n)$ vary slowly over the domain of scattered angles. Therefore, the approximation for the reflection and

transmission coefficients has the similar form to the coefficients for the sound soft scatterer. The proposed processors are expected to perform reasonably well for both types of boundary conditions on the surface of the scatterer.

The numerical simulations were performed for sound hard circular target of radius $L = 1$. The measured field was simulated as the solution to the integral equation obtained by Nystrom method. The mode filtering described in this Section was performed by least-squares method. Eleven receivers placed at the range $x = 30$ from the target were employed in all simulations.

The comparison of two types of the proposed processors has been performed for various values of frequencies. For the purpose of this comparison, the object was placed inside the water column of width $H = 100$ at the depth of $z_0 = 40$ and was excited by the second incident mode. The results of the localization are summarized in Table 3.1.

Table 3.1 Depth localization. The target is located at $z_0 = 40$

Frequency	Number of propagating modes	Range independent processor	Beamforming processor
.1	3	39.6	49.0
.2	6	40.7	41.2
.3	10	39.5	40.9

The performance of the range independent processor is not influenced by the frequency and the resulting relative localization errors are less than 1.7%. The performance of the beamforming processor improves with the increased number of modes, as the closer approximation for $\delta(z-z_0)$ is achieved with the increased number of terms in the summation given by Eq. (3.5). Another possible advantage of range independent processor over beamforming lies in the fact that the angular dependence in the product of reflection and transmission coefficients is less pronounced than in the case of using the reflection coefficient alone.

In addition, we compare the processor performances for various incident modes. In this case the object is placed inside the water column of width $H = 120$ at the depth of $z_0 = 75$. The frequency is given as $k = .2$ and, therefore, there exist 8 propagating modes in the waveguide. The results of the localization are given in Table 3.2. We note that the results are independent of the incident mode, but the localization by the range independent processor is consistently better.

Table 3.2 Depth localization. The target is located at $z_0 = 75$

Incident mode	Range independent processor	Beamforming processor
1-st	74.71	72.97
2-nd	74.71	72.92
3-rd	74.70	72.8
4-th	74.69	72.62

Therefore, we can conclude that for the low frequency field the proposed range independent processor has a superior performance over beamforming. The low frequency assumption allows to localize the object, but does not represent an interesting case for further research on determination of the object shape. To completely solve inverse problem for the shape of the scatterer it is necessary to consider wide frequency range. Therefore, we employ low frequency methods to locate the target and high frequency methods to determine its shape.

3.2.2 Symmetrical Target

Given a source that can excite a single mode, we are able to localize the symmetric target regardless of the frequency range.

Suppose that the m-th incident mode is excited and is incident on the target. In close proximity of the target this mode is composed of two plane waves propagating in the directions $d_{m1} = (\cos\theta_m, \sin\theta_m)$ and $d_{m2} = (\cos\theta_m, -\sin\theta_m)$. The reflection

coefficient for the n-th mode of the scattered field can be represented as

$$\begin{aligned} 2ika_n\sqrt{k_n}R_{nm} &= C_1 e^{iq_n}(A(-d_{n1}, d_{m1}) + A(-d_{n1}, d_{m2})) \\ &+ C_2 e^{-iq_n}(A(-d_{n2}, d_{m1}) + A(-d_{n2}, d_{m2})) \end{aligned} \tag{3.9}$$

where $A(-d_n, d_m)$ is the far field pattern of the scattered field produced by the plane wave incident in the direction d_m and measured in the direction $-d_n$.

For the n-th incident mode, the reflection coefficient of the m-th mode of the scattered field is given as

$$\begin{aligned} 2ika_m\sqrt{k_m}R_{mn} &= C_1 e^{iq_m}(A(-d_{m1}, d_{n1}) + A(-d_{m1}, d_{n2})) \\ &+ C_2 e^{-iq_m}(A(-d_{m2}, d_{n1}) + A(-d_{m2}, d_{n2})) \end{aligned} \tag{3.10}$$

From the reciprocity relation for the scattered amplitude [9], we obtain $A(-d_{m1}, d_{n1}) = A(-d_{n1}, d_{m1})$. Furthermore, if we assume the target to be symmetrical with respect to the x-axis, then $A(-d_{m1}, d_{n2}) = A(-d_{n1}, d_{m2})$ and $A(-d_{m2}, d_{n2}) = A(-d_{n1}, d_{m1})$. Therefore,

$$\begin{aligned} 2ika_m\sqrt{k_m}R_{mn} &= A\Psi_n(z_0) \\ 2ika_n\sqrt{k_n}R_{nm} &= A\Psi_m(z_0) \end{aligned} \tag{3.11}$$

where $A = A(-d_{m1}, d_{n1}) + A(-d_{m2}, d_{n1})$.

To obtain the vertical coordinate z_0, we define the processor as follows:

$$a_m\sqrt{k_m}r_{mn}\Psi_m(z_0) - a_n\sqrt{k_n}r_{nm}\Psi_n(z_0) \tag{3.12}$$

The processing difference is minimized by the least squares method. The same procedure can also be applied to determine the vertical coordinate of the target symmetrical with respect to the line that crosses the x-axis at the angle $\theta_i + \triangle\theta/2$. The numerical simulations were conducted for low frequency $k = .2$ and for intermediate frequency of $k = 3.3$. For the case of low frequency, the water column

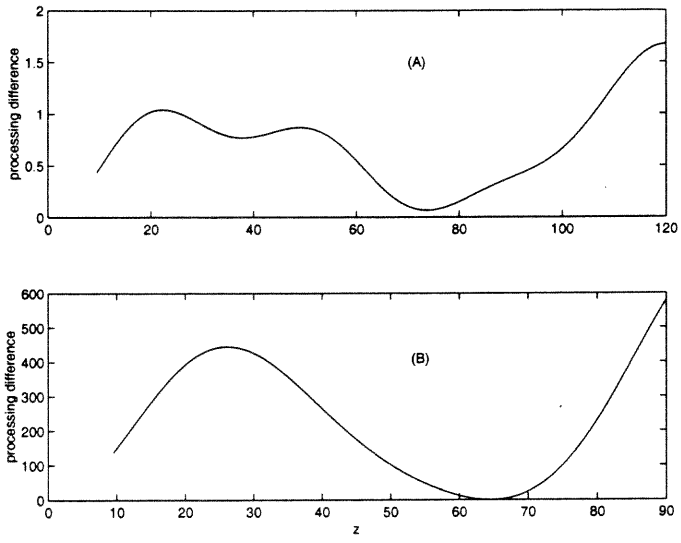

Figure 3.1 The processing difference for symmetrical target. (A) $k = .2$ and $z_0 = 75$; (B) $k = 3.3$ and $z_0 = 65$.

has the width $H = 120$ and the target is located at $z_0 = 75$, for the case of intermediate frequency $H = 100$ and $z_0 = 65$. The object was located at $z = 73.8$ for low frequency field, and at $z = 64.5$ for intermediate frequency field. The resulting processing difference is plotted in Figure 3.1. Due to the periodic nature of the eigenfunctions, it is not feasible to include the high order modes into the minimizing function. The simulations show that the minimization over the first four modes in case of $k = .2$ and the first three modes in case of $k = 3.3$ results in the absolute error of less than 1.6% and .7%, respectively.

3.3 High Frequency Approach to Shape Reconstruction

In this section, we consider an application of high frequency methods to the inverse problem in a waveguide. The information about the shape of the object is embedded into the far field pattern. If we are able to retrieve the far field pattern from the

reflection and transmission coefficients, we can then apply an appropriate method from a variety of methods available for the shape reconstruction in the free space.

The reflection coefficients for an arbitrary target are given in Eq. (3.9). Every reflection coefficient depends on 4 values of the far field pattern at different incident and measured directions, since every mode is represented as a sum of two plane waves with different direction of propagation. Therefore, the amount of information about the free space far field pattern carried in the values of reflection and transmission coefficients is larger for waveguides with higher number of propagating modes. To increase the number of propagating modes, we excite the target by the incident mode of high frequency.

In this work, we limit our consideration to high frequency methods. We adapt the geometrical and physical optics methods of solution of the free space inverse problem to the inverse problem in a waveguide. We should, nevertheless, note that, despite the obvious advantages of high frequency methods in application to the given problem, this approach requires extensive mode filtering. We assume that we can measure reflection and transmission coefficients and that the location of the scatterer is known or has been obtained by the methods of Section 3.2. We also scale all spatial variables by the characteristic size of the target.

First, we apply the method of geometrical optics to the target shape reconstruction. In the geometrical optics limit the far field pattern is given by

$$A(\theta,\beta)=\frac{\sqrt{\sin\frac{\theta-\beta}{2}}}{\sqrt{2G}}e^{ikx(\cos\beta-\cos\theta)+ikz(\sin\beta-\sin\theta)} \tag{3.13}$$

where (x,z) is an unknown specular point on the target contour., and G is a curvature at that point.

In the free space, the contour of the target is obtained from the measurements of the amplitude [29] or phase [30] of the field in the backscattered direction. In a bounded environment of a waveguide, the scattered field is represented as a sum of the propagating modes. The substitution of expression (3.13) into Eq. (3.9) for the

reflection coefficient of the n-th scattered mode excited by the n-th incident mode results in

$$R_{nn} = \frac{1}{\sqrt{2}} C_1 e^{i\lambda_n z_0} \left(\frac{e^{2ikr_{P1}\cos(\theta_{P1}-\beta_n)}}{\sqrt{G_{P1}}} + \frac{\sqrt{\cos\beta_n}\, e^{2ikr_S \cos\beta_n}}{\sqrt{G_S}} \right) + \frac{1}{\sqrt{2}} C_2 e^{-i\lambda_n z_0} \left(\frac{e^{2ikr_{P2}\cos(\theta_{P2}-\beta_n)}}{\sqrt{G_{P2}}} + \frac{\sqrt{\cos\beta_n}\, e^{2ikr_S \cos\beta_n}}{\sqrt{G_S}} \right) \tag{3.14}$$

where $P1$ and $P2$ are the specular points on the target contour for the backscattered direction of the incident plane waves and S is a fixed point where the horizontal inclinations of the incident and reflected rays are equal. The geometry of the target is illustrated in Figure 3.2. The target contour is described as $r = r(\theta)$, the coordinate of the specular point P is $r_P = r(\theta_P)$. If the contour is symmetrical with respect

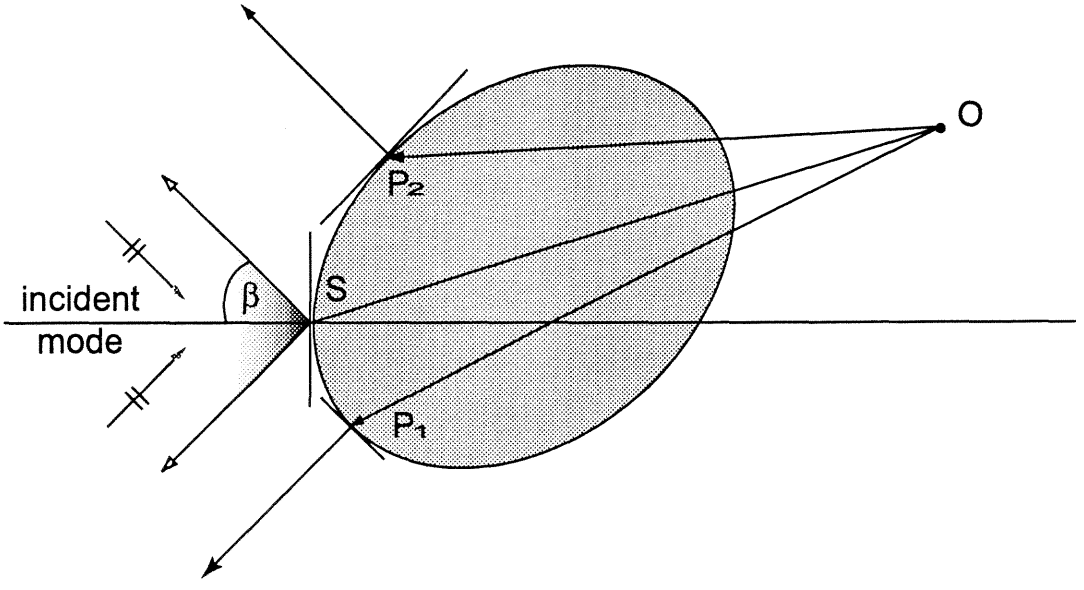

Figure 3.2 Target geometry.

to the horizontal axis, then $r_{P1} = r_{P2}$ and $G_{P1} = G_{P2}$. For the symmetrical contour the reflection coefficient is given as

$$R_{nn} = \frac{1}{\sqrt{2}} \Psi_n(z_0) \left(\frac{e^{2ikr_P \cos(\theta_P-\beta_n)}}{\sqrt{G_P}} + \frac{\sqrt{\cos\beta_n}\, e^{2ikr_S \cos\beta_n}}{\sqrt{G_S}} \right) \tag{3.15}$$

For high range of frequencies the lower order propagating modes have very small angles of inclination, i.e. $\beta_1 \approx 0$. Therefore, for the first propagating mode

$$R_{11} = \frac{2}{\sqrt{2}}\Psi_1(z_0)\frac{e^{2ikr_s}}{\sqrt{G_S}} \tag{3.16}$$

The measurements of the amplitude of this coefficient provide the value of the curvature at point S. The radial coordinate of point S is obtained from the phase of this reflection coefficient.

Therefore, we can determine the amplitude and the phase of the free space scattered field in the backscattered direction as

$$\begin{aligned} |A_{BS}(P_n)| &= |\frac{R_{nn}}{\Psi_n(z_0)} - \frac{\sqrt{\cos\beta_n}}{2}\frac{R_{11}}{\Psi_1(z_0)}| \\ Phase(A_{BS}(P_n)) &= Phase(\frac{R_{nn}}{\Psi_n(z_0)} - \frac{\sqrt{\cos\beta_n}}{2}\frac{R_{11}}{\Psi_1(z_0)}) \end{aligned} \tag{3.17}$$

Due to the presence of many propagating modes, the specular points P_n are densely packed, and, therefore, the expressions given by Eq. (3.17) can be approximated by a smooth function of β. The shape of the target can then be reconstructed by free space methods from the amplitude or the phase of the far field pattern in backscattered direction.

Physical optics represents another high frequency technique that can be applied to reconstruction of the target in free space from the backscattered far field pattern [31]. We employ the physical optics approximation for the scattered field and develop the method to retrieve the shape of the non-symmetrical body inside the waveguide.

In the physical optics limit, the approximation for the scattered field is given as

$$u^s \sim 2\int_L u^{inc}\frac{\partial G}{\partial n}ds \tag{3.18}$$

where L is the side of the body Ω illuminated by the incident wave $u^{inc} = e^{ikx\cdot I}$ with $I = (\cos\beta, \sin\beta)$. In the far field

$$u^s \sim \frac{\sqrt{2}e^{-i\frac{\pi}{4}}}{2\sqrt{\pi}}k\int_L e^{ikx\cdot(\hat{I}-\hat{r}(\theta))}(\hat{r}(\theta)\cdot\hat{n})\,ds\frac{e^{ikr}}{\sqrt{kr}} \tag{3.19}$$

Therefore, for the physical optics approximation the scattering amplitude $A(\theta, \beta)$ is given as

$$A(\theta, \beta) = Ck \int_L e^{ikx\cdot(\hat{I}-\hat{r}(\theta))}(\hat{r}(\theta)\cdot\hat{n})\, ds \tag{3.20}$$

The reflection coefficients of the field scattered from the non-symmetrical body located at (x_0, z_0) are given by Eq. (3.10). For the case of the constant sound speed the reflection coefficient R_{nn} for the n-th mode excited by the n-th incident mode is described as

$$\begin{aligned} 2k_n R_{nn} &= C_1 e^{ik\sin\beta_n z_0}(A(-I, I) + A(-I, I')) \\ &+ C_2 e^{-ik\sin\beta_n z_0}(A(-I', I) + A(-I', I')) \end{aligned} \tag{3.21}$$

where $I = (\cos\beta_n, \sin\beta_n)$, and $I' = (\cos\beta_n, -\sin\beta_n)$ with $\cos\beta_n = \frac{k_n}{k}$ and $\sin\beta_n = \frac{\lambda_n}{k}$. The coefficients C_1 and C_2 are determined from the eigenfunction for the waveguide. In our case of sound soft upper boundary and sound hard lower boundary $C_1 = -C_2 = \frac{\sqrt{2}}{2}$.

After the substitution of Eq. (3.20) into Eq.(3.21) and using the reciprocity condition for the far field patterns $A(-I, I') = A(-I', I)$, we determine

$$\begin{aligned} \frac{2k_n R_{nn}}{C} &= kC_1 e^{i\lambda_n z_0}\Big(\int_{I\cdot n>0}((-I\cdot n)e^{2ikx\cdot I} + (-I'\cdot n)e^{ikx\cdot(I+I')}\Big) \\ &+ kC_2 e^{-i\lambda_n z_0}\Big(\int_{I'\cdot n>0}((-I\cdot n)e^{ikx\cdot(I+I')} + (-I'\cdot n)e^{2ikx\cdot I'}\Big) \end{aligned} \tag{3.22}$$

The coefficient for the n-th scattered right mode can be obtained by sending the n-th incident mode from the opposite side of the body and measuring the reflected field as

$$\begin{aligned} \frac{2k_n \bar{R}_{nn}}{C} &= kC_1 e^{i\lambda_n z_0}\Big(\int_{I\cdot n<0}((I'\cdot n)e^{-2ikx\cdot I'} + (I\cdot n)e^{-ikx\cdot(I+I')}\Big) \\ &+ kC_2 e^{-i\lambda_n z_0}\Big(\int_{I\cdot n<0}((I'\cdot n)e^{-ikx\cdot(I+I')} + (I\cdot n)e^{-2ikx\cdot I}\Big) \end{aligned} \tag{3.23}$$

We assume that we can place an array of sources sending the single mode onto both sides of the target and filter the corresponding scattered modes. Using the

reflection coefficients of the measured field we can then construct the vector $\vec{d}$ with coefficients given by

$$d_n = \frac{2\sqrt{2}k_n}{C}(r_{nn} + \bar{r}^*_{nn}) \tag{3.24}$$

The analytical representation of measured vector $\vec{d}$ is obtained from the reflection coefficients R_{nn} and $\bar{R}_{nn}$ given by Eqs. (3.22)-(3.23). This representation is arranged into the array D with elements given as

$$\begin{aligned} D_n &= \int\int_\Omega (p \cdot n)(e^{ix\cdot(p+p')-i\lambda_n z_0} - e^{2ix\cdot p+i\lambda_n z_0}) \\ &+ \int\int_\Omega (p' \cdot n)(e^{2ix\cdot p'-i\lambda_n z_0} - e^{ix\cdot(p+p')+i\lambda_n z_0})dxdz \end{aligned} \tag{3.25}$$

where $p = kI$, and $p' = kI'$.

We apply the divergence theorem to Eq. (3.25) to obtain

$$D_n = -2k^2 \int\int_\Omega e^{2ikx\cos\beta_n}[\cos^2\beta_n \sin\lambda_n z_0 + \sin\lambda_n(2z + z_0)]dxdz \tag{3.26}$$

We have assumed that we know the range to the target from the time domain methods. Now, we further assume that by timing the response of the reflected pulse, we know the outer left, x_1 and right, x_2, horizontal coordinates of the target Ω. The target is assumed to be a convex body with the upper contour described by a function $z = f_2(x)$ and the lower contour described by a function $z = f_1(x)$. The functions $f_1(x)$ and $f_2(x)$ are to be determined from our measurements of d_n.

The contour functions are assumed to have trigonometric expansions in the region (x_1, x_2)

$$\begin{aligned} f_1 &= \sum_{n=0}^{M1} a_n \cos\frac{n\pi x}{L} + b_n \sin\frac{n\pi x}{L} \\ f_2 &= \sum_{n=0}^{M2} \bar{a}_n \cos\frac{n\pi x}{L} + \bar{b}_n \sin\frac{n\pi x}{L} \end{aligned} \tag{3.27}$$

where $L = \frac{x_2 - x_1}{2}$,

or polynomial expansions

$$f_1 = \sum_{n=0}^{M1} a_n x^n$$

$$f_2 = \sum_{n=0}^{M2} \bar{a}_n x^n \tag{3.28}$$

The integration of Eq. (3.26) results in the following expression for array D

$$D_n = -2k^2 \quad [\quad \cos^2 \beta_n \sin \lambda_n z_0 \int_{x_1}^{x_2} e^{2ik_n x}(f_2 - f_1) + \frac{1}{\lambda_n} \int_{x_1}^{x_2} \sin \lambda_n (f_1 + f_2 + z_0) \sin \lambda_n (f_2 - f_2) dx] \tag{3.29}$$

The substitution of trigonometric (3.27) or polynomial (3.28) expansions into Eq. (3.29) leads to the nonlinear system of equations $D = d$ to be solved for $2(M1 + M2)$ unknown coefficients $a_n, b_n, \bar{a}_n$, and $\bar{b}_n$.

If the system is overdetermined, i.e. the number of propagating modes N exceeds the desired number of Fourier coefficients in the expansion of the target contour, then it is preferable to minimize the processing difference over the domain of $a_n, b_n, \bar{a}_n$, and $\bar{b}_n$. The processing difference to be minimized is given by

$$P = \sum_{n=1}^{M} |D_n - d_n| \tag{3.30}$$

The minimization is performed by least-squares method, and the resulting values of Fourier coefficients completely determine the shape of the target Ω.

For the purpose of the numerical example, we place the circular body inside the waveguide and obtain the reflection coefficients by solving the integral equation for the field on the body using Nystrom method as described in the previous Chapter. After filtering the simulated values of d_n are calculated by Eq. (3.24).

We assume that the circular object of radius $r = 1$ is placed at $(x_0 = 30, z_0 = 25)$ inside the waveguide of width $y = 50$. We also assume that this object is illuminated by the incident field with frequency $k = 8$. Therefore, there exist 127 propagating modes in the waveguide. We choose to use only first 50 modes in least-squares minimization. Finally, we assume that we have information that the extent of the target is between $(-1, 1)$, and it is rotationally symmetrical over x-axis, i.e. $f_1 = -f_2$.

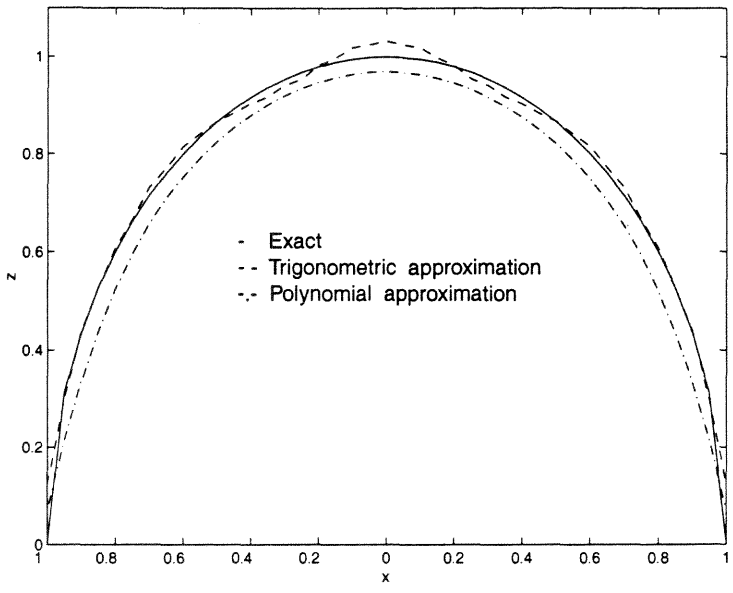

Figure 3.3 The approximate contour of the circular target. $k = 8$

We minimize the functional of Eq. (3.30) by least-squares method to obtain unknown coefficients a_n and b_n. Figure 3.3 shows the resulting shape of the target determined by the above inversion scheme for different types of expansion for the contour of the target. Both types of expansion show good agreement between the simulated and exact contour. For trigonometric expansion, 15 coefficients were determined, while for the polynomial expansion, 9 coefficients were determined. The simulations show that the trigonometric expansion is more sensitive to the change in data, and requires the initial vector of values to be close to the resulting vector.

CHAPTER 4

SCATTERING IN THE WAVEGUIDES WITH MULTIPLE ABRUPT WIDTH TRANSITIONS

4.1 Introduction

In this chapter, we will consider the interaction of the incident plane wave with a flanged waveguide opening into rectangular cavity. The geometry of the problem is shown in Figure 4.1.

Simpler structures with abrupt discontinuities, like flanged waveguide [34, 32], stepped waveguide [33, 35], or double flanged waveguide [38], were considered by many researchers in different areas of application. Numerical [34, 36] and asymptotic [37] techniques were used to obtain the field inside these structures. Solutions of this type of problems are based on the same physical considerations that the field and its' tangential component are continuous across the aperture.

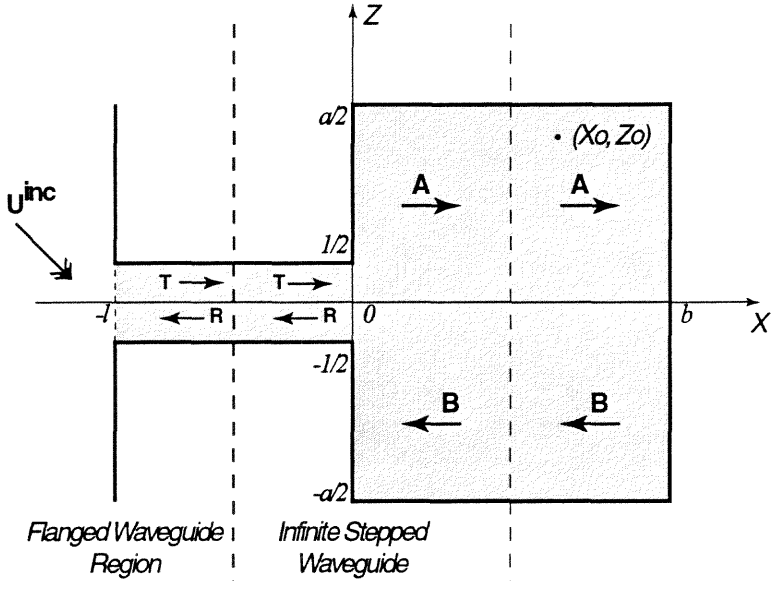

Figure 4.1 Geometry of the structure.

We will employ the above mentioned methods for the simpler structures, and then combine the results for those domains to study the more complex geometry of our problem. Using the scattering matrix approach, we will integrate multiple simple

structures into a single whole structure. To illustrate our approach we will consider two different problems requiring the integration of the following three structures: a flanged waveguide, a channel with abrupt width transition and a rectangular waveguide closed at one end.

First, we will consider the electromagnetic problem. We will study the electromagnetic signals in microwave frequency range propagating in perturbed metallic waveguides. Metallic waveguides are the essential tools in microwave engineering, representing the basic elements of design of such devices as filters, impedance transformers, and ceramic microwave ovens. We will consider the structure shown in Figure 4.1 as the model of the receiver with the waves incident from the exterior coupled to the guided modes of the structure. We will then study the same structure as the dual transmitter model with the line source placed inside the structure. For the electomagnetic problem the field on the walls of the waveguide satisfies Dirichlet's boundary condition.

Next, we will study the acoustic or coastal applications. We will again use the geometric structure shown in Figure 4.1 to model water waves propagating through the entrance channel into the harbor basin. The change of wave height is an important factor in harbor design. For that model, to insure that there is no penetration of the channel walls by the field, we will require Neumann's boundary conditions on the walls. To non-dimensionalize the problem, we choose the channel width W as a characteristic length of the structure, and scale all spatial variables by W: $(x, z) = \frac{(X,Z)}{W}, (a, b, l) = \frac{(A,B,L)}{W}$.

For the purpose of this study, we will consider the incident wave with the wavelength $\lambda \sim 1$. We will also assume that the dimensions of the cavity (a, b) have the same order as the wavelength. Therefore, the asymptotic techniques do not apply to this situation, and we will rely on mode matching together with S-matrix approach to determine the field in different parts of the structure.

At the beginning of Section 4.2, we provide the formulation of TE waveguide problem and the description of S-matrix method used to obtain the field in the structure. In Section 4.2.1, we give the derivation of the elements of S-matrix. In Section 4.2.2, the results of numerical simulations are presented, and resonant cavity dimensions are discussed. Section 4.3 is devoted to the case when the field in TE waveguide is exited by the source embedded inside the cavity. The superposition principle is applied to decouple this problem. The resulting field in the cavity is presented for changing cavity dimensions. In Section 4.4, we give the formulation of the problem as it applies to the coastal wave model. We then describe the adjustments necessary for the implementation of the method of attack, and discuss the results of numerical studies.

4.2 Formulation of TE Waveguide Problem

To study the electric field in the flanged waveguide opening into rectangular cavity, we limit our consideration to TE modes with $E_y = U$ being the only nonzero component of the electric field.

Referring to the Figure 4.1 we note that the total field in the flanged waveguide is exited by the wave incident from the left of the structure at the angle α, and is given by

$$U^{inc} = u_0 e^{ik((x+l)\cos\alpha + z\sin\alpha)} \tag{4.1}$$

In the flanged waveguide region $(-l < x < 0, -\frac{1}{2} < z < \frac{1}{2}) \cup (x < -l, |z| < \infty)$ and the cavity region $(0 < x < b, -\frac{a}{2} < z < \frac{a}{2})$,
the total field U satisfies Hemholtz equation

$$\nabla^2 U + k^2 U = 0 \tag{4.2}$$

subject to Dirichlet boundary condition $U = 0$ on the walls of the structure.

Inside the channel ($-l < x < 0$), the total field U takes the form

$$U = \sum_{n=1}^{\infty} [R_n e^{-ik_n x} + T_n e^{ik_n x}]\Phi_n \tag{4.3}$$

The eigenfunctions and propagating constants for the channel region are given as

$$\begin{aligned} \Phi_n &= \sqrt{2}\sin n\pi(z + \frac{1}{2}) \\ k_n &= \sqrt{k^2 - (n\pi)^2} \end{aligned} \tag{4.4}$$

For simplicity, we will consider the case of only one propagating mode in the channel, so k_1 is real, and $k_n = i|k_n|$ for $n \geq 2$.

Inside the cavity region, the total field U away from the aperture ($0 < x < l$) is given by

$$U = \sum_{n=1}^{\infty} [A_n e^{i\beta_n x} + B_n e^{-i\beta_n x}]\Psi_n \tag{4.5}$$

where

$$\begin{aligned} \Psi_n &= \frac{\sqrt{2}}{\sqrt{a}} \sin \frac{n\pi}{a}(z + \frac{a}{2}) \\ \beta_n &= \sqrt{k^2 - (\frac{n\pi}{a})^2} \end{aligned} \tag{4.6}$$

and the number of propagating modes in the cavity is M, i.e. β_n are real for $n = 1, ..., M$ and $\beta_n = i|\beta_n|$ for $n \geq M + 1$.

To further simplify our analysis, we make an assumption that l and b are large enough to ensure that the evanescent modes in (4.3) and (4.5) can be neglected on the dotted planes in Figure 4.1. Therefore, Eqs. (4.3) and (4.5) have finite sums with one and M terms respectively.

To determine the unknown set of amplitudes A_n, B_n, R_1, T_1, we use the scattering matrix approach that allows to relate the unknowns by $(M + 1)$ linear equations as follows:

$$T_1 = u_0 s_1 + R_1 g_1 \tag{4.7}$$

$$R_1 = \gamma_1 T_1 + \sum_{n=1}^{M} B_n \tau_n \tag{4.8}$$

$$A_j = t_j T_1 + \sum_{n=1}^{M} B_n r_{nj} \tag{4.9}$$

The transmitted mode in the channel is excited by two components: incident plane wave coming from the left and reflected channel mode coming from the right. Therefore, in Eq. (4.7) s_1 is a transmission coefficient, and g_1 is a reflection coefficient for the left and right flanged waveguide problems respectively.

Equations (4.8) and (4.9) describe the another simplified region, namely a waveguide with abrupt change in width. Here γ_1 is the reflection coefficient due to the mode of strength 1, striking the aperture from the left, and $t = (t_1, ..., t_M)$ are the transmission coefficients due to the same mode. The τ_n and r_{nj} are the transmission and reflection coefficients respectively due to the n-th mode incident upon aperture from the right. In the next section, we will describe the methods to determine these reflection and transmission coefficients for both regions.

To satisfy the boundary condition $U = 0$ on the right wall of the cavity, we require $A_n e^{i\beta_n b} + B_n e^{-i\beta_n b} = 0$. That provides the final equation for the system:

$$B = GA \tag{4.10}$$

where G is a diagonal matrix with elements given as $G_{nn} = -e^{2i\beta_n b}$.

In the matrix representation, a linear system (4.7)-(4.10) can be expressed as

$$\begin{aligned} (I - D\Gamma)\overrightarrow{X_B} &= \overrightarrow{F} \\ \Gamma\overrightarrow{X_B} &= \overrightarrow{X_A} \end{aligned} \tag{4.11}$$

where

$$\overrightarrow{X_A} = \begin{bmatrix} R_1 \\ A_1 \\ \vdots \\ A_M \end{bmatrix}, \quad \overrightarrow{X_B} = \begin{bmatrix} T_1 \\ B_1 \\ \vdots \\ B_M \end{bmatrix}, \quad \text{and} \quad \overrightarrow{F} = \begin{bmatrix} u_0 s_1 \\ 0 \\ \vdots \\ 0 \end{bmatrix} \tag{4.12}$$

$$D = \begin{bmatrix} g_1 & 0 & \dots & 0 \\ 0 & -e^{2i\beta_1 b} & \dots & 0 \\ \vdots & \vdots & \ddots & \vdots \\ 0 & \dots & 0 & -e^{2i\beta_M b} \end{bmatrix} \quad \Gamma = \begin{bmatrix} \gamma_1 & \tau_1 & \dots & \tau_M \\ t_1 & r_{11} & \dots & r_{1M} \\ \vdots & \vdots & \ddots & \vdots \\ t_M & r_{M1} & \dots & r_{MM} \end{bmatrix} \tag{4.13}$$

The system (4.11) is solved by Gaussian elimination, and the coefficients for the left and right propagating modes are obtained for both channel (4.3) and cavity (4.5) regions.

4.2.1 Reflection and Transmission Coefficients for the Flanged and Stepped Waveguides

The approximate values of reflection and transmission coefficients s_1 and g_1 can be found by solving the transmitting and reflecting problems for the flanged waveguide region shown in Fig. 4.1.

For the transmitting problem, the field to the left of the aperture is given by

$$P = U^{inc} + e^{ik(-\bar{x}\cos\alpha + z\sin\alpha)} + u^s \tag{4.14}$$

and the field inside the waveguide can be represented as the sum of normal modes as

$$P = \sum_{n=1}^{\infty} \bar{s}_n e^{ik_n \bar{x}} \Phi_n \tag{4.15}$$

where $\bar{x} = x + l$.

By introducing the Green's function $G(\bar{x}, z, \xi, \eta)$ for the half space that satisfies Dirichlet boundary conditions and using standard arguments, we determine the scattered field on the left ($\bar{x} < 0$) as

$$u^s(\xi, \eta) = \int_{-\frac{1}{2}}^{\frac{1}{2}} P(\bar{x} = 0^-, z) \frac{\partial G}{\partial \bar{x}} dz \tag{4.16}$$

We differentiate equation (4.16) and use the continuity conditions for the field and normal velocity at $\bar{x} = 0$ to obtain

$$-i \sum_{m=1}^{\infty} k_m \bar{s}_m \Phi_m + 2ik\cos\alpha e^{ikz\sin\alpha} = \sum_{m=1}^{\infty} \bar{s}_n \int_{-\frac{1}{2}}^{\frac{1}{2}} G_{x\xi}(x = 0, z, \xi = 0, \eta) \Phi_n(\eta) d\eta \tag{4.17}$$

Finally, we use the orthogonality of the eigenfunctions $\Phi_n(z)$ to arrive at the infinite linear system

$$k_m \bar{s}_m + i \sum_{m=1}^{\infty} \bar{s}_n Z_{nm} = 2k \cos\alpha f_m \tag{4.18}$$

where

$$Z_{nm} = \int_{-\frac{1}{2}}^{\frac{1}{2}} \int_{-\frac{1}{2}}^{\frac{1}{2}} G_{x\xi}(x=0,z,\xi=0,\eta)\Phi_n(\eta)\Phi_n(z)d\eta dz \tag{4.19}$$

is an element of symmetric matrix Z, and the forcing term f given as

$$f_m = \int_{-\frac{1}{2}}^{\frac{1}{2}} e^{ikz\sin\alpha}\Phi_m(z)dz = \frac{2\sqrt{2}\lambda_m(i)^{m+1}}{(k\sin\alpha)^2 - \lambda_m^2} \sin\frac{k\sin\alpha + m\pi}{2} \tag{4.20}$$

To obtain numerical solution for $\bar{s}_n$, the system in Eq. (4.18) is truncated to $N \times N$ system, where $N > M$ is increased until it results in a desirable accuracy. We choose $N = 60$, since our simulations show that it yields less than 0.1% relative error for s_1.

To be able to perform the integration in Eq. (4.19), we choose the following representation for the Green's function

$$G = \frac{1}{2\pi} \int_{-\infty}^{\infty} \frac{1}{2i\omega}(e^{i\omega|x-\xi|} - e^{i\omega(x+\xi)})e^{i\alpha(\eta-z)}d\alpha \tag{4.21}$$

where $\omega = \sqrt{k^2 - \alpha^2}$. This representation is obtained by Fourier transform of Hemholtz equation $\nabla^2 G + k^2 G = \delta(x-\xi)\delta(z-\eta)$ in half space.

Then the elements of matrix Z are given by the integral

$$Z_{nm} = -\frac{i\lambda_m\lambda_n}{\pi} \int_{-\infty}^{\infty} \omega \frac{e^{-i\alpha}(-1)^n - 1}{\alpha^2 - \lambda_n^2} \frac{e^{i\alpha}(-1)^m - 1}{\alpha^2 - \lambda_m^2} d\alpha \tag{4.22}$$

In addition to the symmetry of Z, we also note that $Z_{nm} = 0$ if $n - m$ is an odd number. This reduces the amount of calculations in half. For the rest of the elements, the integration of Eq. (4.22) is performed by Chebyshev quadrature and repeating trapezoidal method.

The reflecting problem for the flanged waveguide is similar. The linear system for the reflection coefficients is determined using the same arguments as above and

is given by

$$k_m \bar{g}_m + i \sum_{m=1}^{\infty} \bar{g}_n Z_{nm} = k_m \delta_{Jm} - i Z_{Jm} \tag{4.23}$$

where J is the number of the mode incident from the right, in our case of one propagating mode $J = 1$.

Due to the change of variables, that translates the aperture at $\bar{x} = 0$ to the aperture at $x = -l$, the reflection and transmission coefficients are transformed into

$$\begin{aligned} g_1 &= e^{2ik_1 l} \bar{g}_1 \\ s_1 &= e^{ik_1 l} \bar{s}_1 \end{aligned} \tag{4.24}$$

The reflection and transmission coefficients for the left and right problems in stepped waveguide are determined by Galerkin method that solves an integral equation for the unknown field in the aperture [39]. It should be noted that our numerical model uses the program by S. Walker to calculate matrix Γ in Eq. (4.11).

4.2.2 Results of Numerical Simulations

In this section, we study the solutions of the Eq. (4.11) for various dimensions of the structure shown in Fig. 4.1. For the case of more than one propagating mode, $M > 1$, the dependence of the amplitudes of propagating modes on the dimensions of the structure is very complex and cannot be obtained explicitly. Therefore, we have to conduct numerical studies in order to attain some understanding as to how the amplitudes of the propagating modes in the cavity depend on the parameters of the system.

As our first example, we consider the cavity of width $a = 2$. This width allows for $M = 3$ propagating modes. The field in the structure is excited by the incident plane wave coming at the angle $\alpha = \frac{\pi}{6}$. The length of the channel is given as $l = 2$, so that the evanescent modes are negligible. In Figure 4.2, we show the magnitude of propagating cavity modes as a function of the length of the the cavity b. We note

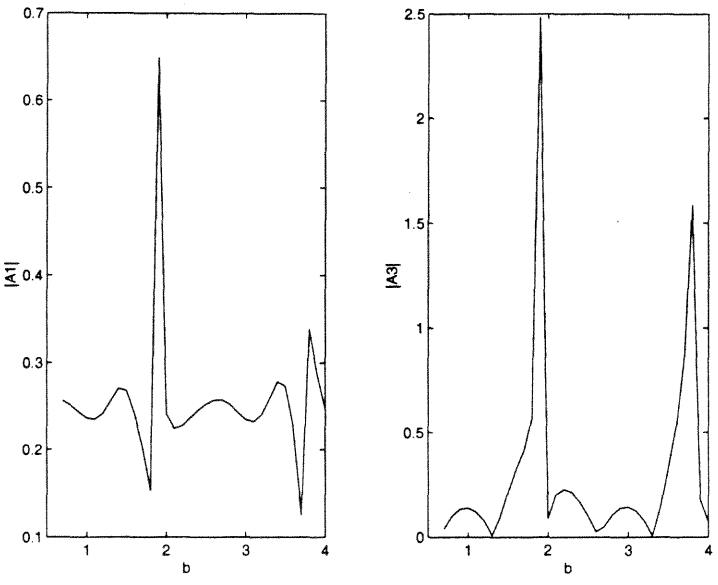

Figure 4.2 The magnitude of coefficients for the first and the third right propagating modes. $a = 2, l = 2, \alpha = \frac{\pi}{6}$

that for "near square" dimensions of the cavity ($b = 1.9$) both the 1-st and the 3-rd modes have a peak in magnitude, though the 3-rd mode is clearly the dominant. The first mode is dominant for $b = 3.3$, where its amplitude has a local peak vs the minimum in the amplitude of the 3-rd mode. We may also note that the next resonant cavity length is found at $b = 2 * 1.9$.

In Figure 4.3, we can see three modes inside the cavity of "near square" dimensions ($a = 2, b = 1.9$). These results are not valid near $x = 0$, since we neglected the effect of the evanescent modes near the aperture. Figure 4.4 pictures the field inside the channel that opens into the cavity.

In Figure 4.5, we show the dependence of the propagating field on the angle of incidence. As expected, the largest amount of energy propagating inside the structure can be attributed to the forward going incident wave, and the propagating energy is steadily decreasing with the increase of the angle of incidence. Figure 4.6 shows that for given dimensions of the cavity there is no noticeable influence of the channel

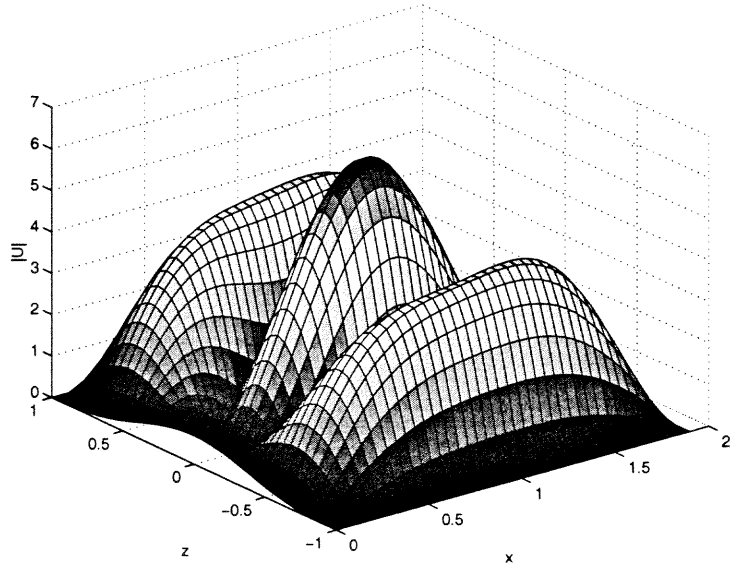

Figure 4.3 The field inside the cavity at resonant dimensions $a = 2, b = 1.9, \alpha = \frac{\pi}{6}$

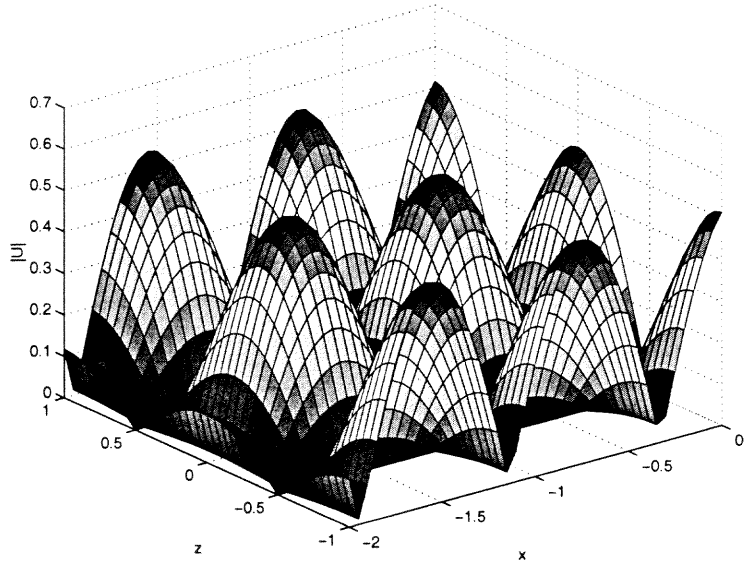

Figure 4.4 The field inside the channel. $a = 2, b = 1.9, l = 2, \alpha = \frac{\pi}{6}$

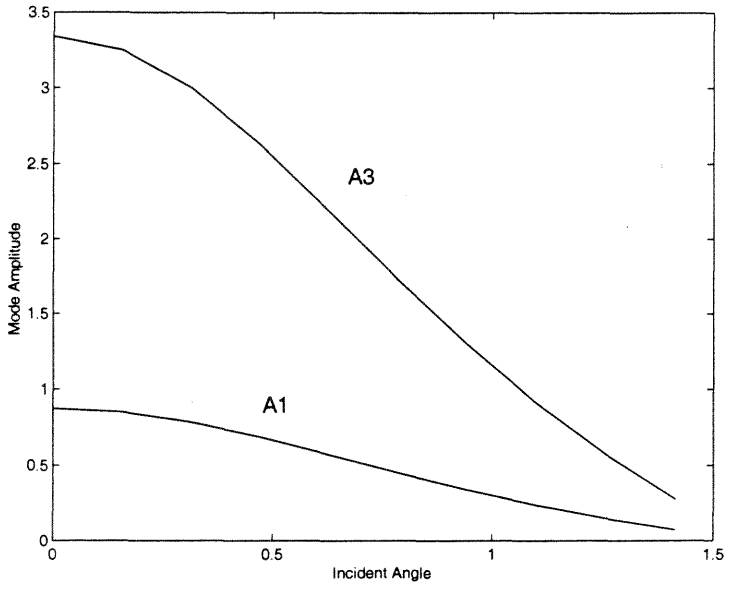

Figure 4.5 The magnitude of coefficients for the first and the third right propagating modes for resonant cavity $(a = 2, b = 1.9)$.

length on the magnitude of propagating modes. We note periodic dependence with slight amplitude variation.

As a second example, we consider the cavity of width $a = 3.5$, so that there exist five $(M = 5)$ propagating modes inside the cavity. The channel length is $l = 3$, the incident wave is inclined at the same angle, $\alpha = \frac{\pi}{6}$, as before. Figure 4.7 presents the magnitude of the propagating modes vs cavity width b. We again notice the clear cases of resonance for the last propagating mode. The resonance occurs at evenly spaced intervals $b_n = b_0 + \triangle n$, where $\triangle = 1.4$ and the first pictured resonant length is $b_0 = 2.9$. We also note that, in contrast with the previous example, "near square" dimensions of the cavity do not produce any dominant modes inside the cavity.

We can conclude from these two examples that there is no simple dependence between the ratio of cavity dimensions and resonant modes, though there clearly exists the repeating variation of the resonant cavity length for any given cavity width.

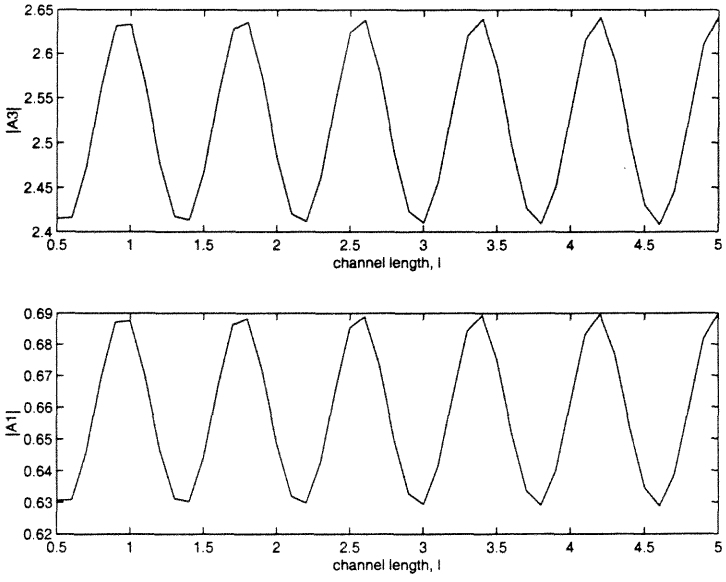

Figure 4.6 The magnitude of the propagating cavity modes vs channel length. $a = 2, b = 1.9$

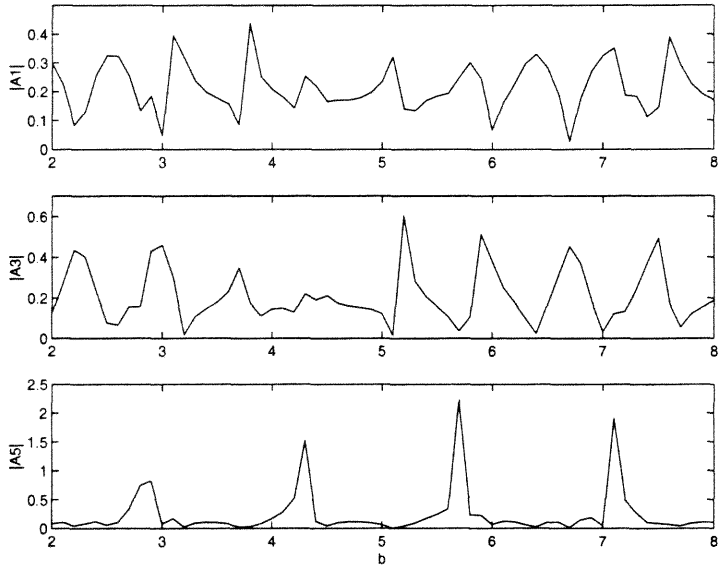

Figure 4.7 The magnitude of coefficients for odd propagating modes. $a = 3.5, l = 3, \alpha = \frac{\pi}{6}$

4.3 Source Inside the Cavity

In this section, we apply the scattering matrix method to evaluate the field excited by the line source placed inside the cavity. To determine the total field U inside the structure we solve Hemholtz equation

$$\nabla^2 U + k^2 U = \delta(x - x_0)\delta(z - z_0) \tag{4.25}$$

where (x_0, z_0) is the location of the source inside the cavity region.

Therefore, U can be expressed in form given by Eq. (4.5). By the superposition principle the field inside the cavity is expressed as a sum of two components

$$U = U_G + U_s \tag{4.26}$$

where U_s is a homogeneous solution, and U_G is a particular solution of Eq. (4.25) in the cavity.

$$U_G = \begin{cases} \sum_{n=1}^{\infty} h_n e^{-i\beta_n x}\Psi_n(z), & x < x_0 \\ \sum_{n=1}^{\infty}(v_n e^{i\beta_n x} + u_n e^{-i\beta_n x})\Psi_n(z), & x > x_0 \end{cases} \tag{4.27}$$

We can neglect the evanescent modes away from the source. Therefore, on the dotted plane to the left from the source shown in Figure 4.1 the coefficients for the propagating modes (A_n and B_n) are determined by solving the linear system of equations

$$\begin{aligned} T_1 &= g_1 R_1 \\ R_1 &= \gamma_1 T_1 + \sum_{n=1}^{M} B_n \tau_n \\ A_j &= t_j T_1 + \sum_{n=1}^{M} B_n r_{nj} \\ B &= GA + h \end{aligned} \tag{4.28}$$

where h is a forcing vector due to the source inside the cavity, given by

$$h_n(x_0, z_0) = \frac{\Psi_n(z_0)}{\beta_n} e^{i\beta_n b} \sin \beta_n(x_0 - b) \tag{4.29}$$

If we have an array of sources located at $x_0 = (x_{01}, \ldots, x_{0L})$ and $z_0 = (z_{01}, \ldots, z_{0L})$, then by superposition principle the forcing term h_n is a sum of contributions from every single source: $h_n = \frac{e^{i\beta_n b}}{\beta_n} \sum_{l=1}^{L} \sin \beta_n (x_{0l} - b) \Psi_n(z_{0l})$.

Since we study the transmitter problem, we focus our attention on the behavior of the field outside of the structure. To satisfy the radiation condition the field exterior to the structure is given by

$$U = \sigma(\theta) \frac{e^{ikr}}{\sqrt{r}}, \quad \text{as} \quad r \to \infty \tag{4.30}$$

By the linearity of the Hemholtz equation, the cross-section σ is given by

$$\sigma(\theta) = \sum_{m=1}^{M} R_m \sigma_T^m \tag{4.31}$$

where R_m is the amplitude of the mode incident on aperture located at $x = -l$, and σ_T^m is a cross-section for the right flanged waveguide problem.

The scattering cross-section σ_T is obtained from Eq. (4.16) using the approximation of the Green's function in the far-field. Using image method to determine the expression for the Green's function, we express its derivative inside the aperture as

$$G_x(x = 0) = -\frac{ik}{2} \cos\theta H_1^{(1)}(k\rho) \tag{4.32}$$

where $\rho = \sqrt{\xi^2 + (\eta - z)^2}$. Therefore, in the far-field

$$G_x(x = 0) = -\frac{i\sqrt{2k}}{2\sqrt{\pi}} e^{i\frac{\pi}{4}} e^{izk\sin\theta} \cos\theta \frac{e^{ikr}}{\sqrt{r}} \tag{4.33}$$

The reflection coefficients for the right problem, g_n, are obtained by the method described in the previous section. After the substitution of Eqs. (4.33) and (4.15) into Eq. (4.16), the scattering cross-section is determined as

$$\sigma_T(\theta) = \sum g_m \frac{2\sqrt{k}\lambda_m (i)^m}{\sqrt{\pi}((k\sin\theta)^2 - \lambda_m^2)} e^{i\frac{\pi}{4}} \sin\left(\frac{k\sin\theta + m\pi}{2}\right) \cos\theta \tag{4.34}$$

The total scattered cross-section is given by

$$\Sigma = \int_{\frac{\pi}{2}}^{\frac{3\pi}{2}} |\sigma(\theta)|^2 d\theta \tag{4.35}$$

and represents the measure of energy radiated into space.

For numerical studies, we have chosen $a = 2$, so that the number of propagating modes is $M = 3$. Figure 4.8 shows the amplitudes of propagating cavity modes due to the field from the source located at $(x_0 = \frac{3b}{4}, z_0 = 0)$. We again see the resonance cavity width at $b = 1.9$.

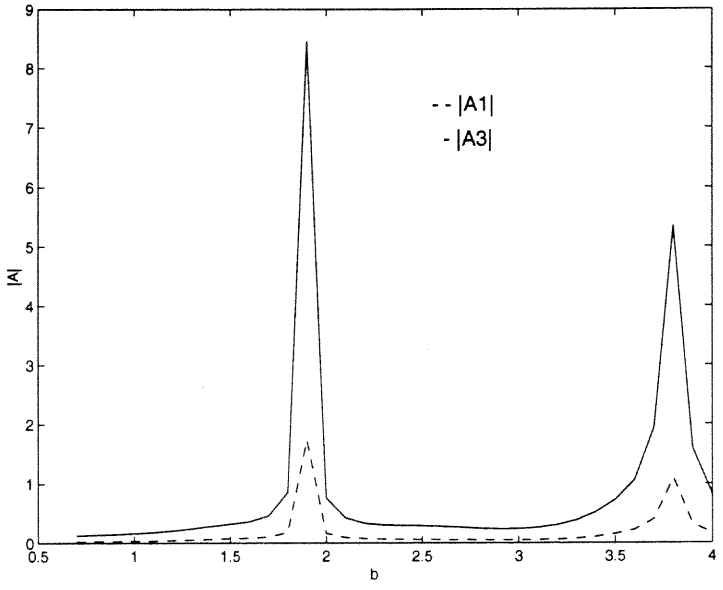

Figure 4.8 The magnitude of propagating modes in the cavity for the source located at $(x_0 = \frac{3b}{4}, z_0 = 0)$.

For this source placement, Figure 4.9 shows the field inside the cavity for the resonant lengths $b = 3.8$ (a), and $b = 3.5$ (b). We can see that at the resonant length the modes are propagating into the channel, while for $b = 3.5$ more energy is trapped inside the cavity.

Figure 4.10 depicts the amplitude of the left propagating mode in the channel and the total cross-section of the scattered field exited by this mode. We can see the correspondence between the peaks of the mode amplitude and the radiated energy. We also note the maximum of radiated energy at the next resonance length of $b = 3.8$.

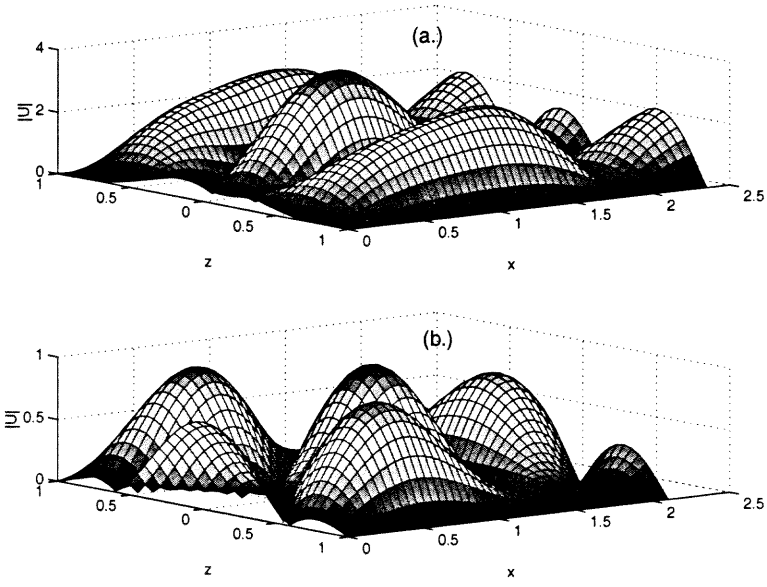

Figure 4.9 Field in the cavity ($x_0 = \frac{3b}{4}, z_0 = 0$). (a) $b = 3.8$, (b) $b = 3.5$

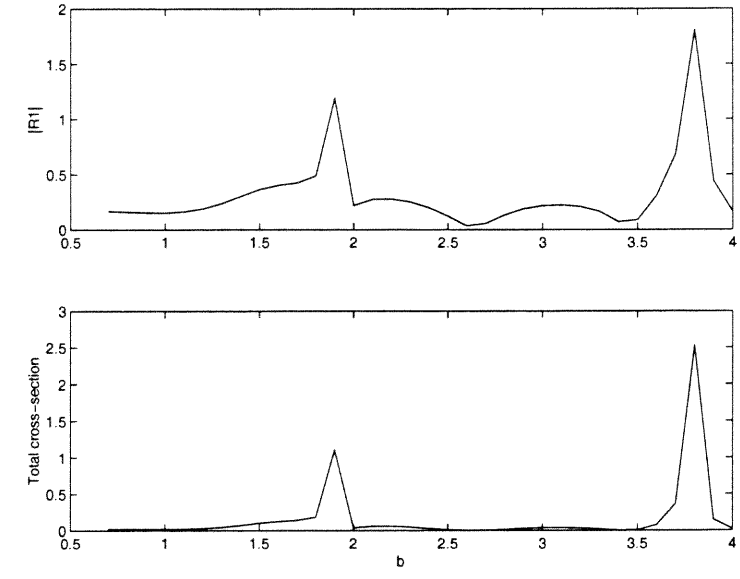

Figure 4.10 The magnitude of the mode in the channel and total cross-section for the source located at ($x_0 = \frac{3b}{4}, z_0 = 0$).

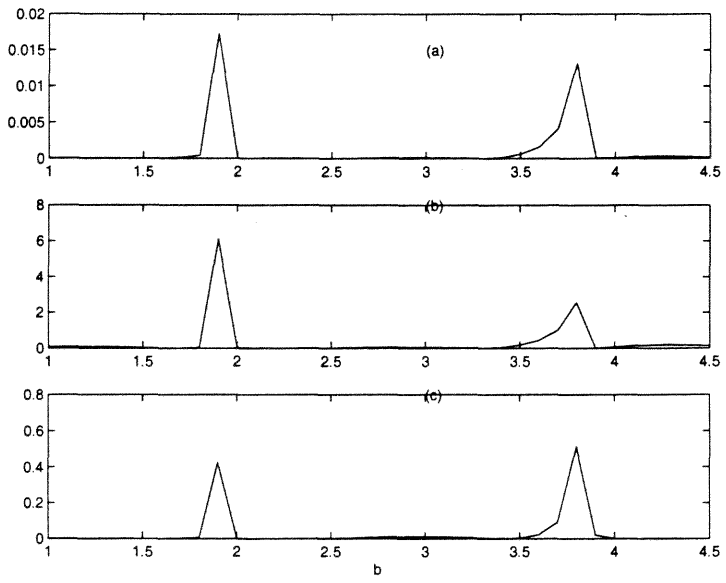

Figure 4.11 Total cross-section. (a) $(x_0 = .8b, z_0 = \pm.99)$, (b) $(x_0 = .8b, z_0 = \pm.5)$, (c) $(x_0 = .9b, z_0 = .8)$.

Figure 4.11 shows the total cross-section of the scattered field for different source placements. The field excited by two vertically symmetrical sources located close to the cavity walls at $(x_0 = .8b, z_0 = \pm.99)$ is shown in Figure 4.11(a). For this source location we can see that very little energy radiates out of the structure. As sources are moved closer to each other (in Figure 4.11(b), $z_0 = \pm.5$), the amount of radiated energy significantly increases. Figure 4.11(c) shows the total cross-section from one source located in the upper left corner of the cavity. We can note resonant dimensions of the cavity at $b = 1.9$ and $b = 3.8$ for all three source locations.

In Figure 4.12, we see the field exited by the source located at $x_0 = .9b, z_0 = .8$. We note clear mode structure of the field inside the cavity of resonant length $b = 3.8$. Figure 4.12(b) shows the energy trapped inside the cavity of dimensions $a = 2, b = 3$.

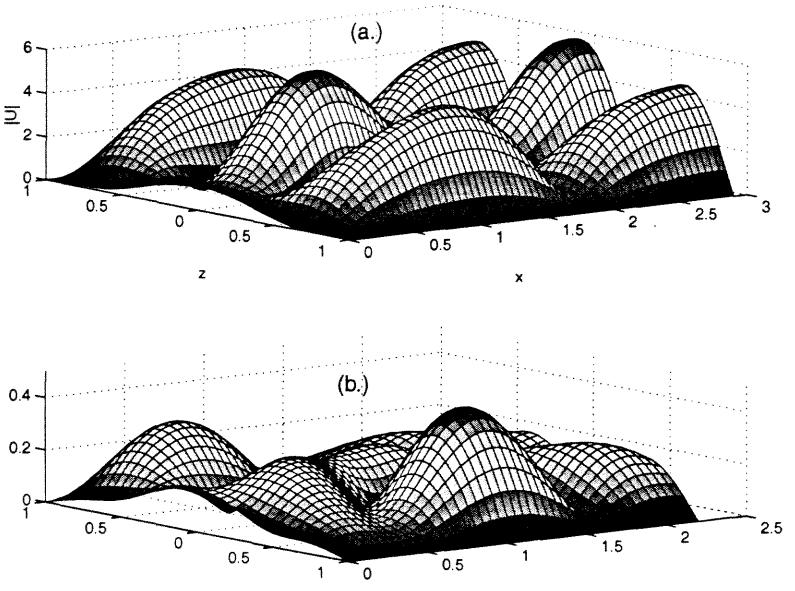

Figure 4.12 Field in the cavity ($x_0 = .9b, z_0 = .8$). (a) $b = 3.8$, (b) $b = 3.0$

4.4 Coastal Wave Model

In this section, we consider the model for water waves propagating through the entrance channel into the closed harbor. The geometry of the problem is the same as described in Section 4.2. Assuming the constant water depth, the velocity potential of the wave field satisfies Hemholtz equation (4.25) and Neumann boundary conditions on the walls of the structure.

As derived in Section 4.2, the potentials are described by modal expansion Eqs. (4.3)-(4.5) with the eigenfunctions given as

$$\begin{aligned} \Phi_n &= \epsilon_n \cos n\pi(z + \frac{1}{2}); \quad \epsilon_n = 1 \ (n = 0), \quad \epsilon_n = \sqrt{2} \ (n \geq 1) \\ \Psi_n &= \bar{\epsilon_n} \cos \frac{n\pi}{a}(z + \frac{a}{2}); \quad \bar{\epsilon_n} = \sqrt{\frac{1}{a}} \ (n = 0), \quad \bar{\epsilon_n} = \sqrt{\frac{2}{a}} \ (n \geq 1) \end{aligned} \tag{4.36}$$

The unknown coefficients of the propagating modes are obtained by solving linear system (4.11). The elements of the system matrix are determined by solving left and right problems for the flanged and stepped waveguide with hard boundary conditions.

For the flanged waveguide region, the solutions for the reflection and transmission coefficients are determined by truncated normal mode analysis using Green's function approach. The reformulation of the left and right problems as linear algebra problems is described by G. Kriegsmann [32]. The necessary translation of the aperture to the location $x = -l$ is reflected in Eq. (4.25).

The reflection and transmission coefficients for the left and right problems in the infinite stepped waveguide can be described by a variety of methods. It can be easily shown that the integral equation approach [39], Green's function argument [32] or mode matching approach [35] all result in the equivalent linear system of equations for unknown transmission coefficients. The advantage of mode matching technique is that it provides an additional linear system of equations to determine the reflection coefficients without further analysis.

To apply mode matching, we represent the field on the both sides of the aperture as the sum of normal modes, and require that they satisfy two continuity conditions across aperture. This results in two systems of equations that can be solved numerically to obtain unknown coefficients.

Left problem, when the incident mode is coming from the narrow waveguide, is described by

$$\begin{aligned} \beta_p t_p + \sum_{n=0}^{N2} t_n \Big(\sum_{m=0}^{N1} k_m \int \Phi_m \Psi_p \int \Phi_m \Psi_n \Big) &= 2k_J \int \Phi_J \Psi_p \\ \sum_{n=0}^{N2} t_n \int \Phi_m \Psi_n - \delta_{Jm} &= \gamma_m \end{aligned} \tag{4.37}$$

where J is the number of the incident mode Φ_J ($J = 0$, or $J = 1$). In our geometry we have two propagating modes in the channel.

Right problem, when an incident mode is coming from the cavity, is represented by the following system:

$$\tau_l + \sum_{m=0}^{N1} k_m \tau_m \Big(\sum_{n=0}^{N2} \frac{1}{\beta_n} \int \Phi_m \Psi_n \int \Phi_l \Psi_n \Big) = 2 \int \Psi_J \Phi_l$$

$$\frac{\beta_J}{\beta_p}\delta_{Jp} - \frac{1}{\beta_p}\sum_{m=0}^{N1} k_m \tau_m \int \Phi_m \Psi_p \;=\; r_p \tag{4.38}$$

We solve the system of Eq. (4.38) for $J = 1 : M$, where M is the number of propagating modes in the cavity.

Another advantage of employing mode matching approach to the solution of the infinite stepped waveguide problem is that it allows for clearer understanding of how the infinite matrices should be truncated. In systems (4.37),(4.38) $N1$ is the number of modes used in the representation of the field in the channel, $N2$ is the number of modes used in representation of the field in the cavity. Therefore, $N1 \gg 2$ and $N2 \gg M$. To ensure that modes in the channel are matched with the similar modes in the cavity, it is necessary to maintain $N2 > aN1$ [40].

In our numerical study, we first take $a = 2$ as before, corresponding to $M = 3$. To provide for sufficient accuracy, we choose $N1 = 20$, requiring $N2 > 40$ (we choose $N2 = 50$). For the purpose of this example, we select the incident wave

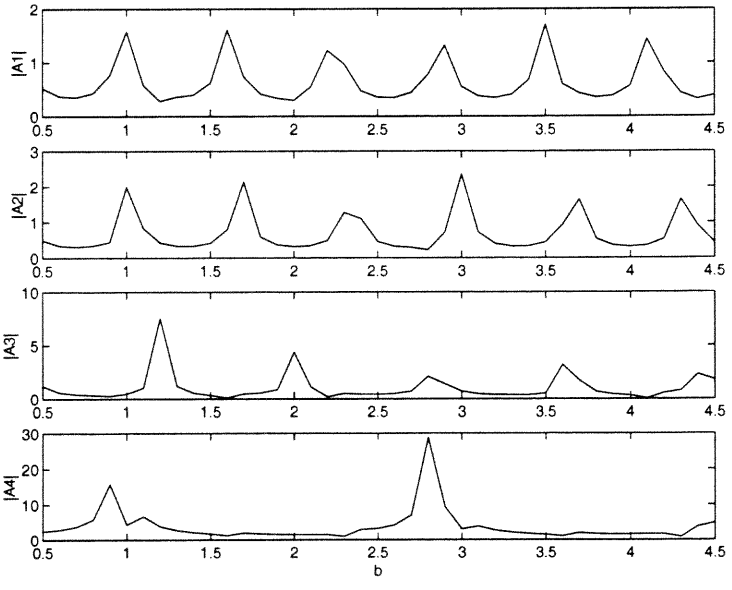

Figure 4.13 The magnitude of the propagating modes in the cavity. $a = 2$.

to be inclined at $\alpha = \frac{\pi}{6}$, and the channel length to be $l = 2$. Figure 4.13 shows the magnitude of right propagating modes in the cavity vs the length of the cavity.

We note that the resonant lengths are evenly spaced for every mode. The intervals between the resonances are increasing with the increasing of the mode numbers, and higher order modes become dominant at their resonant length.

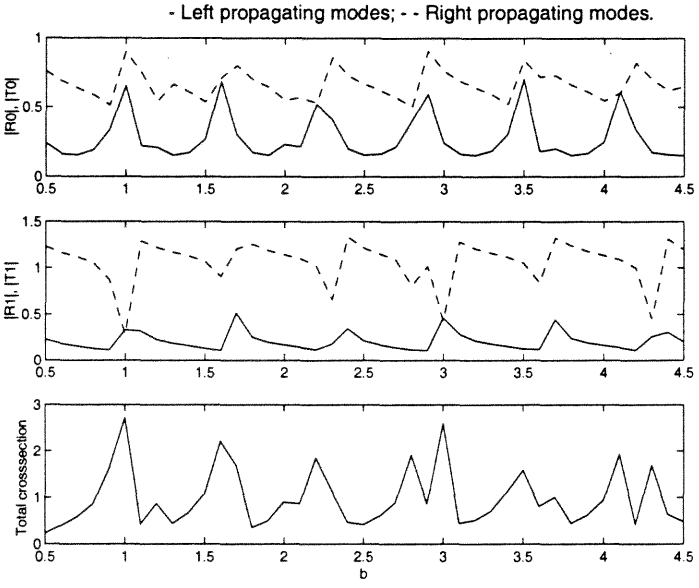

Figure 4.14 The magnitude of the propagating modes in the channel. Total cross-section for $a = 2$ and $l = 2$.

Figure 4.14 depicts the amplitudes of the left and right propagating modes in the channel as a function of cavity length. We see no strong resonance in the channel. Figure 4.14 also shows the total cross-section, given by Eq. (4.35), where $\sigma(\theta) = \sigma_R + \sum_{m=1}^{2} R_m \sigma_T^m$. Total cross-section measures the amount of energy reradiated into space. We note that the peaks of the curve for total cross-section correspond to the different lengths than the resonant lengths of the dominant cavity mode.

Comparing the results of Dirichlet problem, presented in Section 4.2 with Neumann problem of this section, we can conclude that the presence of both symmetric and antisymmetric modes in Neumann problem accounts for more computational complexity of the solution. We also note that Neumann problem results do not lend themselves to interpretation as clearly as the results of Dirichlet problem.

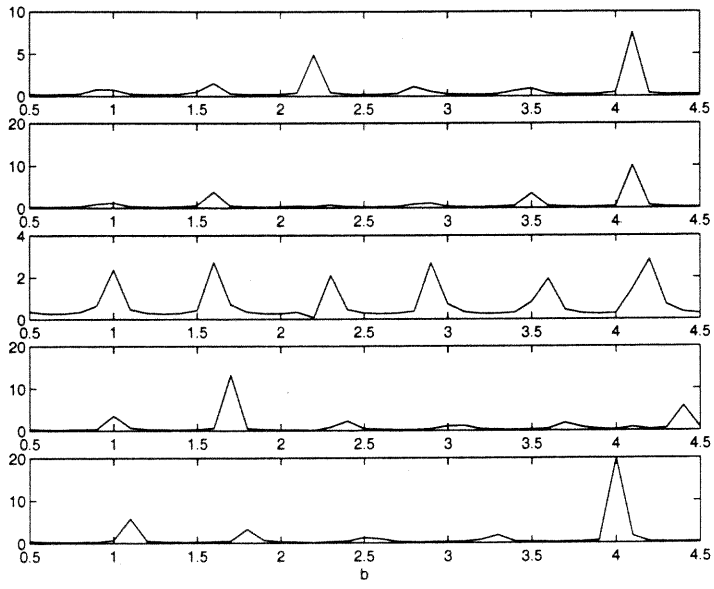

Figure 4.15 The magnitude of even numbered propagating modes in the cavity ($|A0|$ on the top, and $|A8|$ on the bottom). $a = 10$.

In our next example, we increase the size of the cavity to $a = 10$. This results in increase of the number of propagating modes to $M = 15$. To maintain the same accuracy of the representation of the field in the channel ($N1 = 20$), we now have to use $N2$ bigger than 200 for the left and right infinite stepped waveguide problems. Figure 4.15 shows the magnitude of the modes numbered from 0 through 8, and Figure 4.16 shows the magnitude of the modes numbered from 1 through 9. As the number of modes increases, it becomes more difficult to determine the dominance of any single mode. However, some modes (as mode number 7) stay sub-dominant at any length of the cavity.

Increasing the size of the cavity to $a = 50$, leads to the increase in the number of propagating modes to $M = 79$. To maintain the same level of accuracy, we now need $N2$ to be greater than 1000. For $a = 50$, the scattering matrix contains 6241 elements. Most of these elements are determined as a solution of 1000×1000 system of equations, rendering the numerical calculation impractical.

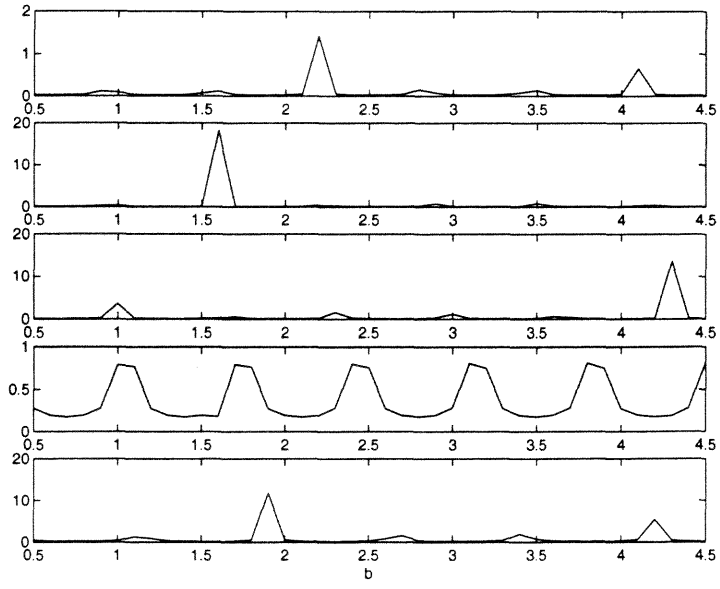

Figure 4.16 The magnitude of odd propagating modes in the cavity. ($|A1|$ on the top, and $|A9|$ on the bottom). $a = 10$.

The number of propagating modes in the cavity is directly proportional to the height of the cavity, a. The number of modes in the expansion for the infinite stepped waveguide problem is also directly proportional to a. Thus, the computational complexity of the coastal model is at least of the order of a^4. Therefore, for cavities with dimensions $a \gg 1$ it becomes necessary to develop an alternative approach to the solution of the field inside the given structure.

CHAPTER 5

APPROXIMATE METHOD TO DETERMINE THE FIELD INSIDE LARGE CAVITIES

5.1 Introduction

We have seen in Chapter 4 that extensive numerical calculations are required to accurately approximate the scattered field inside the geometrical structure pictured in Figure 4.1. The complexity of the calculations increases with the increase of the size of the cavity, straining computer resources. Therefore, it is of interest to develop an approximate model with numerical complexity independent of the size of the cavity. This can be accomplished by taking into account the length scales of the given problem.

We will employ the asymptotic techniques to analyze the field scattered by the given structure. Methods of physical optics are efficient when $W \gg \lambda$ [37], where W is a characteristic length of the structure, chosen as the channel width. For long waves, with $KW \ll \pi$ and $KA \ll \pi$, the scattering inside the infinite stepped waveguide has been studied by Lamb [41]. We will consider the problem with $\lambda \sim W$ and $2\pi > KW > \pi$ that allows for the presence of propagating modes inside the channel. In this chapter, we study scattering inside large cavities $a = \frac{A}{W} \gg 1$. This assumption corresponds to a realistic physical problem in a coastal wave application.

We start by scaling all spatial variables with respect to W and introducing the perturbation parameter $\epsilon = \frac{1}{a}$ to develop an asymptotic approach to the solution of the scattering problem. The idea behind the method described in this chapter is similar to the approach used in Chapter 2. The field (or its tangential component) inside the transition region between two waveguides with different widths (1 and $a \gg 1$) can be approximated by the field inside the aperture of the flanged waveguide. This approximation allows for an easy evaluation of the elements of the scattering

matrix, and can be used to solve the system given by Eqs. (4.11) or (4.28) and to determine the field inside the whole structure.

In Section 5.2 of this chapter, we present the numerical results for the field inside the aperture of the flanged waveguide and for the field in the aperture of the waveguide with abrupt width transition. We then compare these fields to show their increasing similarity with the increase in cavity size. In Section 5.3 we give the theoretical basis for our field approximation for both left and right problems, and discuss its asymptotic bounds. The results obtained by our approximation method and the resonant cavity dimensions are presented in Section 5.4.

5.2 Numerical Comparison of the Fields in the Apertures of Flanged and Stepped Waveguides

In this section, we compare the solutions of the flanged waveguide problem with the solutions of the stepped waveguide problem. We limit our consideration to the case of Dirichlet boundary conditions on the walls of the waveguides.

First, we consider the reflection problem, when the exciting mode originating in a waveguide is incident on the aperture. The method to determine the reflected field in the flanged waveguide is presented in Section 4.2.1. The field inside the aperture is given by

$$P = \sum_{n=1}^{\infty} \bar{g_n} \Phi_n \tag{5.1}$$

The unknown coefficients $\bar{g_n}$ are found by solving the linear system given by Eq. (4.23). To determine the field inside the aperture of the infinite stepped waveguide region of relatively small widths we use the integral equation approach developed by S. Walker [39]. To achieve better accuracy for wider waveguides, Walker's model was modified based on the ideas of mode matching described in Section 4.4 by truncating the infinite sum of the normal mode representation of the field. In addition, to make a computer model feasible, we approximate part of

the infinite sum by an integral. This integral is computed by trapezoidal method, allowing to perform the required summation using bigger step size than the step size defined by the sum in the integral equation method. For both solutions we verify our numerical results using conservation of power law.

For our numerical simulation, we choose $k = 5$, so that only a single mode propagates inside the channel. The incident mode is the first mode coming from the right $U^{inc} = e^{-ik_1 x}\Phi_1(z)$. Figure 5.1 shows the magnitude of the scattered field inside the aperture of the flanged waveguide in comparison with the magnitude of the scattered field in the aperture of the infinite stepped waveguide for $a = 5$ and $a = 25$. Figure 5.2 shows the comparison of the phases of the scattered fields for the same values of width a. Due to the similar physics of the problems, we observe the same form for the scattered fields in all three cases . The field in the infinite stepped waveguide with larger width transition ($a = 25$) is in better agreement with the field in the flanged waveguide, though the discrepancies are still too large to consider them to be in close agreement.

Figures 5.3 and 5.4 show the comparison of the magnitudes and the phases of the reflected fields in the apertures as the transition width a is further increased. For the given value of width a ($a = 150$), we note good agreement of the curves with the maximum relative deviation of less than 5%.

In Figure 5.5, we show the field in the flanged waveguide and the field in the wide stepped waveguide, $a = 150$, for a different value of frequency, $k = 8$. We can see that for this increased frequency two curves almost coincide. We do not have enough data to conclude that better agreement between fields is achieved for the higher values of wavenumber k, but we propose this conjecture.

Next, we model the transmitting problem. Inside stepped waveguide region the exciting mode is incident on the aperture from the wider waveguide. The same exciting mode is incident on the aperture of the flanged waveguide from the open

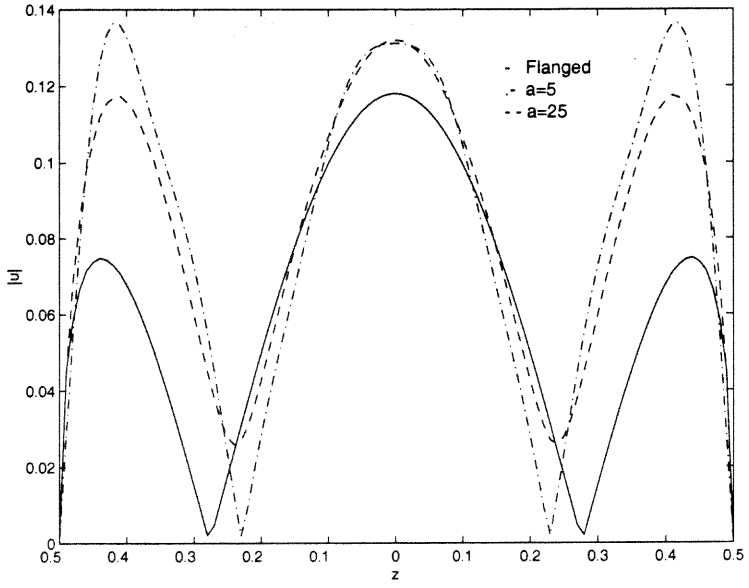

Figure 5.1 The magnitude of the fields inside the aperture.

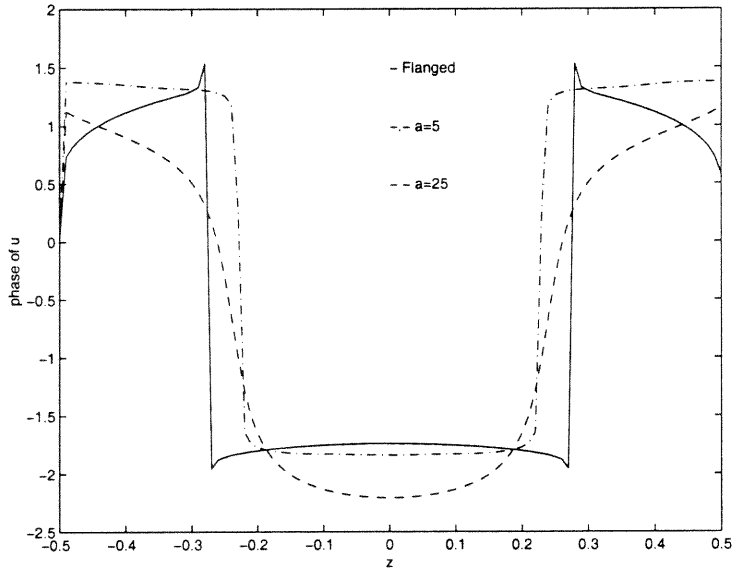

Figure 5.2 The phase of the fields inside the aperture. $k = 5$

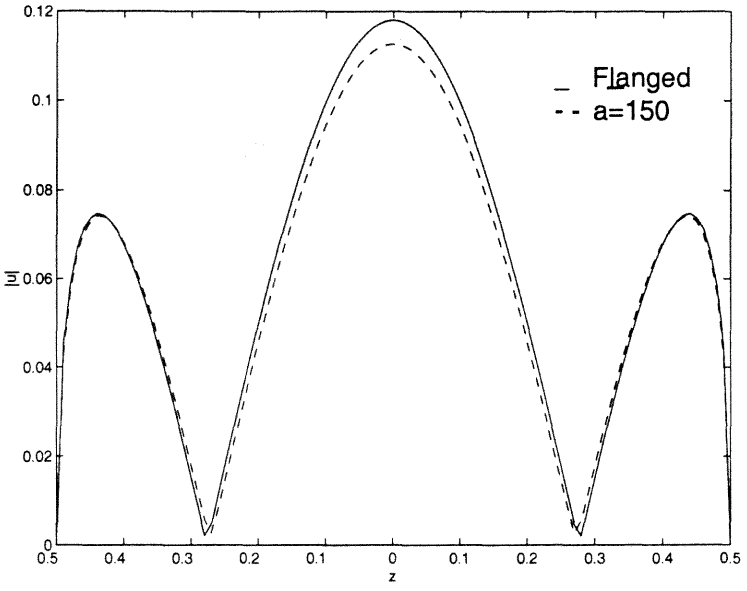

Figure 5.3 The comparison of the field magnitudes inside the aperture for $a \gg 1$.

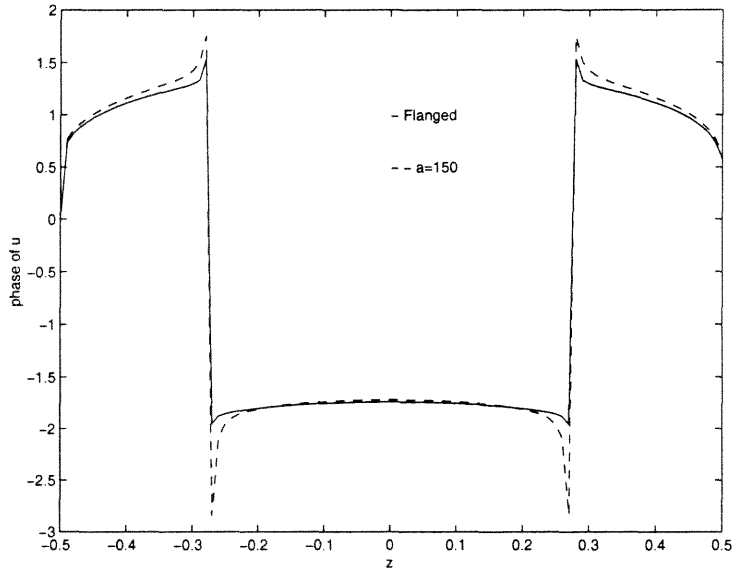

Figure 5.4 The comparison of the field phases inside the aperture for $a \gg 1$. $k = 5$

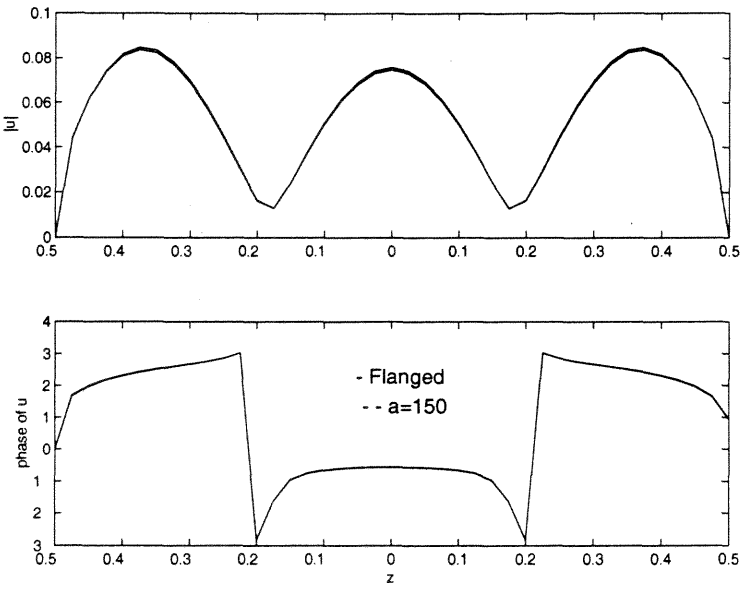

Figure 5.5 The comparison of the fields inside the aperture for $a \gg 1$ and $k = 8$.

space. In our numerical simulation, we compare the fields inside the aperture of the flanged waveguide with the field inside the aperture of the wide stepped waveguide with $a = 150$. The incident mode is chosen as the last propagating mode of wide waveguide, $U^{inc} = e^{-ik_{238}x}\Psi_{238}(z)$. In Figure 5.6, we picture the magnitude and the phase of the fields inside the aperture. We note an excellent agreement between the curves representing the magnitude of the fields, and a slight deviation between the phases. This deviation is likely to be the result of the rounding off procedure for the inverse tangent function, since the deviation in transmission coefficients of the scattered fields is of the order of 10^{-5}.

Therefore, from our numerical example we can conclude that the field in the aperture of the infinite stepped waveguide with $a \gg 1$ can be approximated by the field in the aperture of the flanged waveguide. In the next section, we will derive the asymptotic bounds of this approximation.

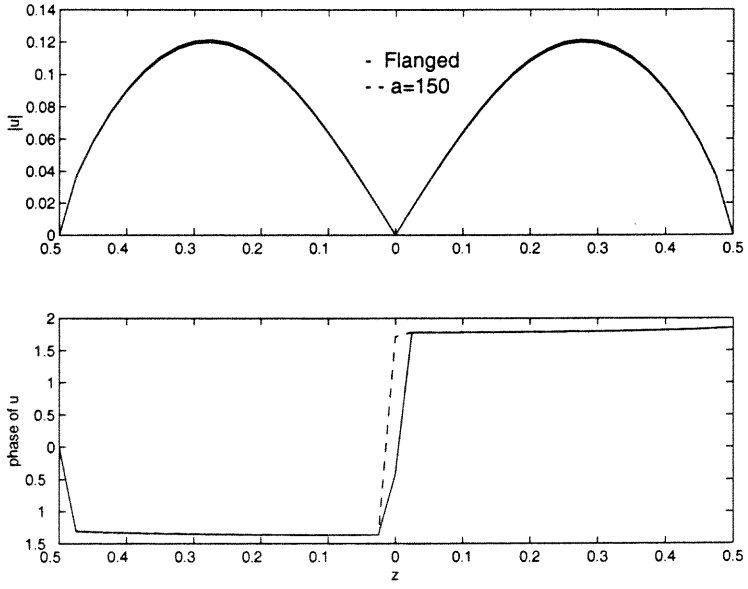

Figure 5.6 The comparison of the fields inside the aperture for transmitting problem. $k = 5$.

5.3 Approximation of the Field Inside the Aperture of the Stepped Waveguide

In order to approximate the field inside the aperture of the stepped waveguide by the field inside the aperture of the flanged waveguide, we have to demonstrate how accurate the approximation is and under what conditions it is valid. In the previous section we have showed numerically that the fields inside the aperture tend to agree better for the higher values of the transition width a and wavenumber k. In this section, we will show the reason behind this behaviour of the fields. We will also demonstrate asymptotically how the difference between the fields inside the aperture depends on the size of the stepped waveguide and the frequency of the wave. We will then determine an asymptotic bound for the difference of the fields for reflecting and transmitting problems.

We again limit our consideration to the case of Dirichlet boundary conditions on the walls of the waveguides. It should be noted, however, that the same asymptotic method with slight modifications can be applied for Neumann boundary conditions.

The solutions to the transmitting and reflecting problem for the flanged waveguide are described in Section 4.2.1. The values of the reflection coefficients g_n are determined by solving linear system

$$(K + iZ)g = (K - iZ)\vec{e_J} \tag{5.2}$$

where K is a diagonal matrix with elements $K_{nn} = k_n = \sqrt{k^2 - \lambda_n^2}$, Z is the matrix with elements given by Eq. (4.22), and $\vec{e_J}$ is a unit vector.

The values of transmission coefficients s_n of the scattered field excited by the mode Ψ_J propagating from the open space are determined by solving linear system

$$(K + iZ)s = 2\beta_J \vec{f} \tag{5.3}$$

where $f_m = \int_{-\frac{1}{2}}^{\frac{1}{2}} \Psi_J \Phi_m dz$.

To obtain the solutions for the stepped waveguide, we employ the integral equation method described by S. Walker [39]. The reflection coefficients are represented as the solutions to the system

$$(K + G)\eta = (K - G)\vec{e_J}, \tag{5.4}$$

For transmission coefficients, the corresponding system is given as

$$(K + G)\varsigma = 2\beta_J \vec{f} \tag{5.5}$$

where G is symmetric coupling matrix given by

$$G_{nm} = \sum_{p=1}^{\infty} \beta_p L_{pm} L_{pn} \tag{5.6}$$

with $L_{pm} = \int_{-\frac{1}{2}}^{\frac{1}{2}} \Psi_m(z)\Phi_p(z)dz$.

We should note that for stepped waveguide region the systems (5.4) and (5.5) result from the normal mode representation of the scattered field. Therefore, the solutions for the reflection and transmission coefficients are valid for $k \neq m\pi$ and $k \neq \frac{m\pi}{a}$ for any m.

From now on, we will only consider the transmitting problem given by Eqs. (5.3) and (5.5), since an identical approach can be used for the reflecting problem of Eqs. (5.2) and (5.4).

The difference between the solutions of linear systems (5.3) and (5.5), s and ς, is described by the theorem on the condition of equations [42]. For any matrix norm, the relative deviation between two solutions is bounded by

$$\frac{\|s-\varsigma\|}{\|s\|} \leq M\|(K+iZ)^{-1}\|\|iZ-G\| \tag{5.7}$$

where M is a constant given as $\frac{1}{1-\alpha}$ with $\alpha = \|(K+iZ)^{-1}(iZ-G)\|$.

If the perturbation $(iZ-G)$ is small enough, then $\alpha < 1$, and the upper bound on the difference $s-\varsigma$ is proportional to the maximum of the norm of the difference between matrices G and iZ. Thus, we will obtain the estimate on the difference $G-iZ$.

After simplification of Eq. (4.22), using the property of odd and even functions, the elements of the matrix iZ are determined as

$$iZ_{nm} = \begin{cases} 4\frac{\lambda_n\lambda_m}{\pi}\int_0^\infty \frac{\omega}{(\alpha^2-\lambda_n^2)(\alpha^2-\lambda_n^2)}(1-(-1)^n\cos\alpha)d\alpha, & n-m = \text{even} \\ 0, & n-m = \text{odd} \end{cases} \tag{5.8}$$

where $\lambda_n = n\pi$, and $\omega = \sqrt{k^2-\alpha^2}$.

The elements of matrix G are given by Eq. (5.6). After performing the integration, we find nonzero elements of G as

$$G_{nm} = \frac{8\lambda_n\lambda_m}{a}\sum_p \frac{\beta_p}{(\lambda_n^2-(\frac{p\pi}{a})^2)(\lambda_m^2-(\frac{p\pi}{a})^2))}(1-(-1)^n\cos\frac{p\pi}{a}), \quad \text{if } n-m = \text{even} \tag{5.9}$$

While $G_{nm} = 0$, if $n-m$ is odd.

The summation in Eq. (5.9) is performed over even values of p, if n and m are even, and over odd values of p, if n and m are odd, since L_{ij} is zero for odd $(i-j)$. We will consider the difference $|G_{nm}-iZ_{nm}|$ for even values of n and m. The same

derivation applies for odd values. The summation of Eq. (5.9) over even numbers can be expressed as

$$\begin{aligned} G_{nm} &= \frac{4\lambda_n\lambda_m}{\pi}\triangle[S_1 + iS_2] \\ &= \frac{4\lambda_n\lambda_m}{\pi}\triangle[\sum_{p=0}^{N}\frac{\sqrt{k^2-x_p^2}(1-\cos x_p)}{(\lambda_n^2-x_p^2)(\lambda_n^2-x_p^2)} + i\sum_{p=N+1}^{\infty}\frac{\sqrt{x_p^2-k^2}(1-\cos x_p)}{(\lambda_n^2-x_p^2)(\lambda_m^2-x_p^2))}], \end{aligned} \tag{5.10}$$

where $\triangle = \frac{2\pi}{a}$, $x_p = \triangle p$, and $N = [\frac{k}{\triangle}]$.

The real part of Eq. (5.11) can be approximated by Euler-Maclaurin sum formula as

$$S_1 = \int_0^{x_N} f(\alpha)d\alpha + \frac{1}{2}\triangle(f(0) + f(x_N)) + \frac{\triangle^2}{12}f'(x_N) + O(\triangle^3) \tag{5.11}$$

where $f(\alpha) = \frac{\sqrt{k^2-\alpha^2}(1-\cos\alpha)}{(\lambda_n^2-\alpha^2)(\lambda_n^2-\alpha^2)}$.

We note that if $x_N = k$, i.e. $\frac{p\pi}{a} = k$, then the approximation of the sum by an integral fail, as $f'(x_N) \to \infty$.

Since $\int_0^{x_N} f(\alpha)d\alpha = \int_0^k f(\alpha)d\alpha - \int_{x_N}^k f(\alpha)d\alpha$, where $\int_0^k f(\alpha) < f(x_N)\triangle$, we can bound the deviation between the series and the integral as follows:

$$|S_1 - \int_0^k f(\alpha)d\alpha| < \frac{1}{2}\triangle|f(x_N)) - \frac{\triangle}{16}f'(x_N)| + O(\triangle^3) \tag{5.12}$$

The imaginary part of Eq. (5.11) is approximated by Euler-Maclaurin formula for infinite n as

$$S_2 \sim \int_0^k f(\alpha)d\alpha + E \tag{5.13}$$

where $|E| < \frac{1}{2}\triangle|f(x_{N+1})) - \frac{\triangle}{16}f'(x_{N+1})|$.

Therefore, the difference between the matrix elements of G and iZ is bounded by

$$|G_{nm} - iZ_{nm}| < \frac{2\sqrt{2}\lambda_n\lambda_m}{a}C + O(\triangle^3) \tag{5.14}$$

where C is the maximum between $|f(x_N)) - \frac{\triangle}{16}f'(x_N)|$ and $|f(x_{N+1})) - \frac{\triangle}{16}f'(x_{N+1})|$.

Based on this bound, we can conclude that for the lower propagating modes, such that $n, m \ll a$, the difference between the matrix elements is of the order $\frac{1}{a}$. For

higher order modes, such that n or $m \sim a$, $f(x_N)$ and $f'(x_N)$ have order $O(\frac{1}{n^2m^2})$, and, therefore, the difference between the matrix elements is of the order $\frac{1}{a^3}$.

The accuracy of the approximation of the series S_1 and S_2 by the integrals is implicitly dependent on the frequency k. As k approaches $\frac{l\pi}{a}$ for any l, the derivative $f'(x_N)$ approaches $\frac{1}{\sqrt{k^2-(\frac{l\pi}{a})^2}}$. Therefore, the contribution of $\frac{\triangle^2}{6}f'(x_N)$ becomes the dominant contribution for the error of the approximation. As k is fixed in the middle of the range between $\frac{l\pi}{a}$ and $\frac{(l+1)\pi}{a}$ for some given l, the dependency of the error of the approximation on frequency is more complex. We have studied the behaviour of the quadrature estimate of the error, given by $E_{nm}(k) \approx k\triangle\frac{\sum^{N(k)} f'_p(\alpha,k)}{N(k)}$, as a function of frequency k. This function is not monotone, and it has different local extremums as we vary indices n and m.

The same procedure is also applicable to Neumann boundary conditions on the walls of the structure. The difference between transmission or reflection coefficients is bounded by the matrix norm of the difference between the Galerkin matrix G and matrix iZ. The elements of matrices G and iZ for Neumann boundaries are given as

$$\begin{aligned} G^{(N)}_{nm} &= \frac{8}{ia}\sum_{l=1}^{\infty}\frac{(l\pi)^2(1-(-1)^l\cos x_p)}{a^2\beta_l(\lambda_n^2-x_p^2)(\lambda_n^2-x_p^2)} \\ iZ^{(N)}_{nm} &= \frac{4}{i\pi}\int_0^{\infty}\frac{\alpha^2(1-(-1)^m\cos\alpha)}{\omega(\lambda_n^2-x_p^2)(\lambda_n^2-x_p^2)}d\alpha \end{aligned} \tag{5.15}$$

Using the same argument as above we can show that $\|G - iZ\| = O(\frac{1}{a})$.

5.4 Field Inside the Harbor

In this section, we present the method to determine the field inside the harbor of large characteristic dimensions. The geometry of the problem is shown in Figure 4.1. We assume that the size of the harbor A is much larger than the width of the entrance channel, i.e. $a = \frac{A}{W} \gg 1$.

In Section 4.4, we used the scattering matrix approach to determine the field inside the harbor with dimensions comparable with the width of the entrance channel. It was shown that if the size of the harbor becomes relatively big compared to the width of the channel, the evaluation of scattering matrix elements by the methods of Section 4.4 tends to be infeasible. To evaluate the elements of the scattering matrix, given by Eq. (4.13), we will approximate the field inside the aperture of the stepped waveguide by the field inside the aperture of the flanged waveguide. Once the scattering matrix has been evaluated, the linear system (4.11) can be solved and the field inside the harbor can then be determined.

For transmission problem on the stepped waveguide region, the field in the narrow waveguide is given as

$$P_1 = u^{inc} + \sum \gamma_n e^{-ik_n x} \Phi_n(z), \tag{5.16}$$

and the field in the wider waveguide is represented as

$$P_2 = \sum t_m e^{i\beta_m x} \Psi_m(z), \tag{5.17}$$

where γ_n and t_m are unknown coefficients to be used in scattering matrix Γ. The incident wave u^{inc} is the mode coming from the narrow waveguide, $u^{inc} = e^{ik_J x}\Phi_J$.

To determine the unknown coefficients γ_n and t_m, we solve the corresponding transmission problem for the same incident mode in the flanged waveguide region, and obtain the reflection coefficients α_n. We then approximate the field inside the aperture of the stepped waveguide by the field field inside the aperture of the flanged waveguide. Therefore, the scattered field inside the aperture is now given as $u = \sum \alpha_n \Phi_n(z)$. Then the scattered field in the narrow waveguide is approximated by u, as x approaches 0^-.

$$(P_1 - u^{inc})(x = 0) = \sum \gamma_n \Phi_n(z) = \sum \alpha_n \Phi_n(z) \tag{5.18}$$

Using the orthogonality of mode functions Φ_n, we obtain the reflection coefficients for the stepped waveguide region as

$$\gamma_n = \alpha_n \tag{5.19}$$

The continuity condition of the velocity across aperture is given as

$$\sum_m \beta_m t_m \Psi_m(z) = k_J \Phi_J - \sum_n k_n \gamma_n \Phi_n(z) \tag{5.20}$$

Using zero boundary condition for the velocity on the walls of the structure together with orthogonality of Ψ_n in the harbor, we obtain the following solution for the transmission coefficients:

$$t_m = \frac{1}{\beta_m}(k_J \int \Phi_J \Psi_m - \sum_{n=1}^{N} \alpha_n k_n \int \Phi_n(z)\Psi_m(z)dz \tag{5.21}$$

For the case of reflection problem in the stepped waveguide, the field in the narrow waveguide is expressed as

$$P_1 = \sum \tau_n e^{-ik_n x}\Phi_n(z), \tag{5.22}$$

and the field in the wider waveguide is given as

$$P_2 = u^{inc} + \sum r_m e^{i\beta_n m x}\Psi_m(z), \tag{5.23}$$

The incident mode is coming from the wider waveguide, $u^{inc} = e^{-i\beta_J x}\Psi_J$. The field inside the aperture is approximated by the field in the aperture of the flanged waveguide for the same incident mode $u = \sum \bar{\alpha}_n \Phi_n$. We apply the orthogonality of the modes and continuity condition to determine the approximation for the transmission and reflection coefficients as:

$$\begin{aligned} \tau_n &= \bar{\alpha}_n \\ r_m &= \delta_{Jm} - \frac{1}{\beta_m}\sum_{n=1}^{N} \bar{\alpha}_n k_n \int \Phi_n(z)\Psi_m(z)dz \end{aligned} \tag{5.24}$$

From Eqs. (5.21) and (5.24) it follows that in order to evaluate the elements of $M \times M$ scattering matrix, where M is a number of propagating modes, we need to obtain solutions for the flanged waveguide problem. These solutions are determined by solving $N \times N$ linear system, where N is independent of the size of the harbor. We maintain $N = 60$ for all our numerical models derived in Chapters 4 and 5.

For the purpose of our numerical simulation, we send a water wave with wavelength $26m$ into the channel of length $124m$ and width $20.7m$. The channel enters large $2482m$ wide harbor. The scaling with respect to channel width non-dimensionalizes the data to $k = 5$, $l = 6$, and $a = 120$. For these dimensions of the harbor, we have two modes in the entrance channel and 191 mode in the harbor basin.

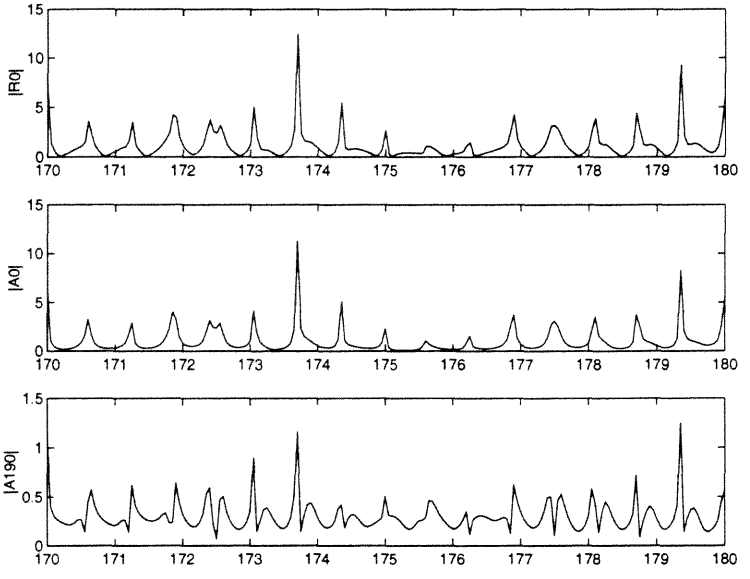

Figure 5.7 The magnitude of the propagating channel and harbor modes.

In Figure 5.7, we depict the magnitude of dominating modes in the channel, R_0, and in the harbor, A_0 and A_{190}. We note that the standing mode dominates the higher order modes. We also see that these zero order modes in the channel and harbor almost perfectly match each other. The remaining energy is redistributed among the other modes. Due to the computational complexity of the problem, we

limited the range of the length of the harbor to [170, 180], and located resonances in this range. We can see two resonant lengths at $b = 173.7$ and $b = 179.35$ in both channel and harbor regions.

Figure 5.8 shows the field inside the harbor of resonant dimensions $a = 120$, $b = 179.3$. We note the pattern of standing waves propagating inside the harbor basin. Due to the scattering matrix method used to obtain the field, the representation of the field is not accurate near $x = 0$. Nevertheless, we can clearly see a broadening channel inside the harbor with almost no field within the channel. The waves disperse away from this shadow region.

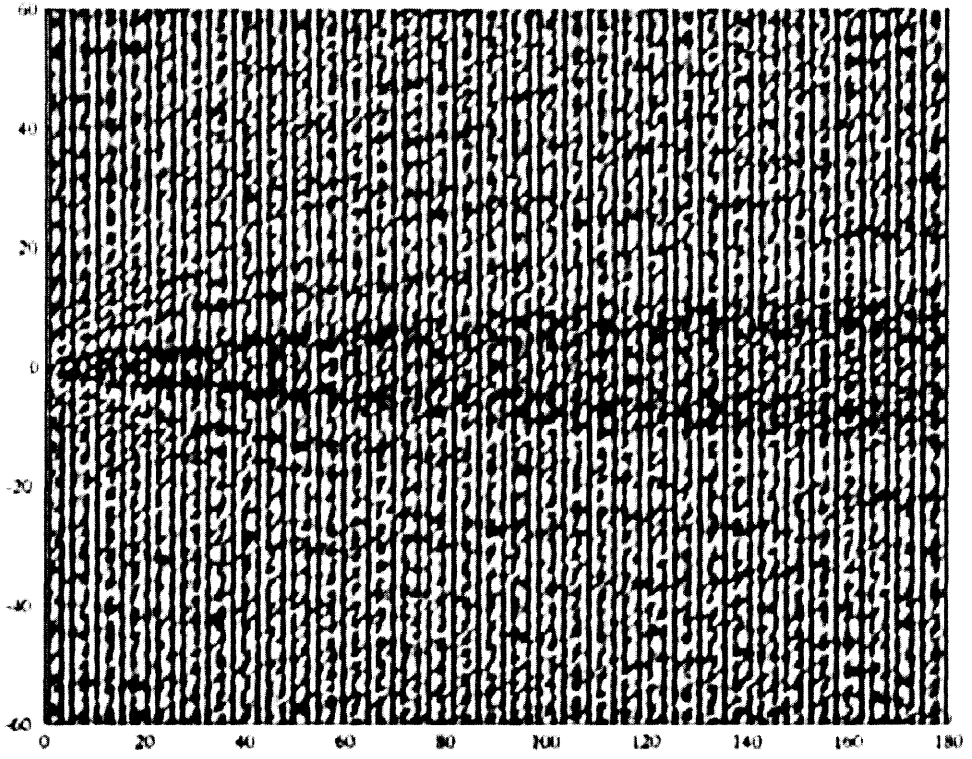

Figure 5.8 The field inside the harbor of length $b = 179.35$.

The development of the calm region in the middle of the harbor can be explained by the following argument. The field in the harbor is excited by the modes coming through the entrance channel. The first mode can be decomposed into two plane waves that strike the opposite corners of the aperture at the same angles. The

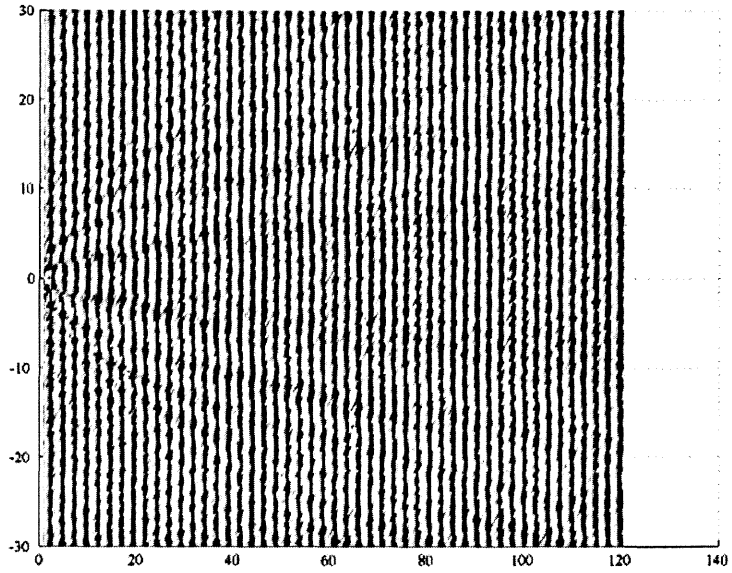

Figure 5.9 The field inside the harbor of length $b = 173.7$.

waves diffracted off the opposite corners are similar to each other in frequency and magnitude but differ in phase. Due to this phase shift, the superposition of these two diffracted fields can interfere and cancel each other inside the region bordered by two outgoing plane waves representing the incident mode.

Figure 5.9 shows the field inside the harbor basin for another resonant length of $b = 173.7$. To be able to see wave pattern more clearly, we pictured only the central part of the harbor. For this harbor width, we can also note the shadow channel in the middle of the harbor, however, the field is now present inside the channel. This field is due to the reflections from the boundaries of the harbor.

Figures 5.9 and 5.8 demonstrate that the method presented in this Chapter produces physically plausible results for the field inside the harbor of large dimensions. The asymptotic approximation employed in this method allowed us to cut the amount of calculations by nearly a^4.

CHAPTER 6

FUTURE RESEARCH

6.1 Acoustic Applications

In Chapter 2 of this dissertation, we have applied an asymptotic approximation of the field on the surface of the small body submerged inside the waveguide by the field on the body in free space. We have shown that if the object is located close to one of the waveguide boundaries the field on the body can be approximated by the field in the half space. As a topic for future study, it might also be interesting to consider the case where the small object is located directly at the waveguide surface and is treated as a perturbed boundary. The applicability of the suggested asymptotic techniques to this case remains to be investigated.

In Chapter 3, we have considered the solutions to the inverse problem in the waveguide. The shape reconstruction of the target was performed by high frequency methods. It remains to be investigated whether the free space far field pattern can be obtained from the scattered field measured in the waveguide and, therefore, if well-developed free space methods for any frequency can be applied to retrieve the shape of the body. Another proposed avenue for the future study is to adjust the regularization methods of the free space valid in the intermediate frequency range for the case of scattering inside wide waveguides.

6.2 Electromagnetic and Harbor Design Applications

The geometry studied in Chapters 4 and 5 can be considered as a prototype for an electromagnetic transmitter or a marine harbor. In both areas of application, it is imperative to understand the resonance conditions to achieve an efficient design.

We have studied the methods allowing to obtain the solution for the scattered field inside the given structure. We have also used the numerical simulations to determine the resonant dimensions of the structure. In order to gain a better

understanding of the resonance effects, more efficient approach to evaluation of the resonant dimensions of the structure remains to be developed. The development of the systematic approach to the study of the resonance is a subject of future research.

APPENDIX A
METHOD OF MATCHED ASYMPTOTICS

Two scales, represented by the characteristic size of the submerged object and the depth of the waveguide, are introduced. Different scales suggest decoupling of the problem and using inner and outer asymptotic expansions. The scaling with respect to the characteristic length constitutes the inner problem, analogous to free-space scattering. For the outer problem, scaled by the depth of the waveguide, the solution away from the object is obtained by normal modes method. The matching region, where both asymptotic expansions are valid, is determined. The inner expansion in the far-field and exact Green's function for the waveguide are calculated on an arbitrary circular surface inside the matching region. The integration around this surface results in an easy expression for reflection and transmission coefficients for the scattered modes in terms of the radiating pattern, defined by the shape of convex object. Easy modifications can be made, as the object is close to one of the boundaries, to account for multiple scattering between them. The outline for these modifications is presented. In addition, the normal mode solution for the scattered field used in the model does not neglect the continuous spectrum and, therefore, accurately presents redistribution of the energy among all modes. The submerged object is not required to be located in the far-field of the source, as in previously mentioned models, leading to the reduction of noise in the incident field and increase in the accuracy of the model.

The solution to the outer problem is given by Eq. (2.3). To obtain the inner problem we dimensionalize variables with respect to the size of the object $\bar{x} = \frac{x'-x'_0}{L}, \bar{z} = \frac{z'-z'_0}{L}$. Now the size of the target is $O(1)$. If we assume that the submerged object is not close to one of the boundaries, then the boundaries of the waveguide have the vertical coordinates of $O(\epsilon^{-1})$ and, therefore, the problem is reduced to the free space scattering. The index of refraction in the inner region $n'(z') = n(\epsilon\bar{z} + z_0)$ is

approximated by $n(z_0) = n_0$. Then the solution for the scattered field is represented by the integral equation of the first kind. For the approximation $n \sim n_0$ to be valid, we assume that the condition $\rho \ll \epsilon^{-1}$ is satisfied. Then in the far field, $\rho \gg 1$, u^s simplifies to

$$u^s \sim CA(\theta)\frac{e^{i\bar{k}n_0\rho}}{\sqrt{\bar{k}\rho}}, \tag{A.1}$$

where $C = i\frac{\sqrt{2}}{4\sqrt{\pi}}e^{-i\frac{\pi}{4}}$, and vectors $\vec{x} = (\bar{x}, \bar{z})$, $\hat{r}(\theta) = (\cos\theta, \sin\theta)$.

The region where both solutions are valid, if one exists, allows to determine the correspondence between the reflection or transmission coefficients and the radiating pattern. Since the outer expansion is valid away from $(0, 0)$, and the inner expansion is valid for ρ, such that

$$1 \ll \rho \ll \frac{1}{\epsilon}, \tag{A.2}$$

the common region is described by the Eq. (A.2) in terms of the inner variable, or by $\epsilon \ll r \ll 1$, where $r = \sqrt{(x - x_0)^2 + (z - z_0)^2}$, in terms of the outer variable.

We choose small value of δ, so that the circle of radius $r = \delta$ around the body belongs to the matching region. Then the matched solution can also be determined as

$$u^s(\zeta, \eta) = \delta \int_0^{2\pi} (u^s \frac{\partial G}{\partial r} - G\frac{\partial u^s}{\partial r})d\theta \tag{A.3}$$

where G is the Green's function for the outer problem, given by Eq. (2.9), and u^s is the far-field inner approximation of the scattered field on the circle of radius $\rho = \frac{\delta}{\epsilon}$ around the body.

After substitution of determined asymptotic expressions into Eq. (A.3), the scattered field can be found as

$$u_1^s \sim \begin{cases} \delta C\frac{e^{iy}}{\sqrt{y}}\sum_{n=0}^{N}\frac{i\Psi_n(\eta)}{2ka_n\sqrt{k_n}}e^{ika_n(\zeta - x_0)}[C_1e^{ikq_0}\cdot I_1 + C_2e^{-ikq_0}\cdot I_2] & \text{if } x < \zeta \\ \delta C\frac{e^{iy}}{\sqrt{y}}\sum_{n=0}^{N}\frac{i\Psi_n(\eta)}{2ka_n\sqrt{k_n}}e^{ika_n(x_0 - \zeta)}[C_1e^{ikq_0}\cdot I_3 + C_2e^{-ikq_0}\cdot I_4] & \text{if } x > \zeta \end{cases} \tag{A.4}$$

where $y = \dfrac{\bar{k}n_0}{\epsilon}$,

$$
\begin{aligned}
I_1 &\sim \int_0^{2\pi} A(\theta) e^{iy\hat{r}(\theta)\cdot\hat{r}(\pi-\theta_n)} \left(\frac{i\bar{k}n_0}{\epsilon} - \frac{i\bar{k}n_0}{\epsilon}\hat{r}(\theta)\cdot\hat{r}(\pi-\theta_n)\right) d\theta \\
I_2 &\sim \int_0^{2\pi} A(\theta) e^{iy\hat{r}(\theta)\cdot\hat{r}(\theta_n+\pi)} \left(\frac{i\bar{k}n_0}{\epsilon} - \frac{i\bar{k}n_0}{\epsilon}\hat{r}(\theta)\cdot\hat{r}(\theta_n+\pi)\right) d\theta \\
I_3 &\sim \int_0^{2\pi} A(\theta) e^{iy\hat{r}(\theta)\cdot\hat{r}(\theta_n)} \left(\frac{i\bar{k}n_0}{\epsilon} - \frac{i\bar{k}n_0}{\epsilon}\hat{r}(\theta)\cdot\hat{r}(\theta_n)\right) d\theta \\
I_4 &\sim \int_0^{2\pi} A(\theta) e^{iy\hat{r}(\theta)\cdot\hat{r}(-\theta_n)} \left(\frac{i\bar{k}n_0}{\epsilon} - \frac{i\bar{k}n_0}{\epsilon}\hat{r}(\theta)\cdot\hat{r}(-\theta_n)\right) d\theta
\end{aligned}
$$

Since large parameter $y \gg 1$ is present in the phase of the integrals, they are evaluated asymptotically by the method of stationary phase. Each integral has two stationary points: $P_1 = \pi - \theta_n$ and $P_2 = -\theta_n$ for I_1 and I_4; $P_1 = \theta_n$ and $P_2 = \pi + \theta_n$ for I_2 and I_3.

The first order of asymptotic approximation for the scattered field in the waveguide is now obtained and expressed as

$$
u_1^s \sim \begin{cases} -C\sqrt{2\pi}e^{i\frac{\pi}{4}} \displaystyle\sum_{n=0}^{N} \frac{\Psi_n(\eta) e^{ika_n(\zeta-x_0)}}{ka_n\sqrt{k_n}} [C_1 A(-\theta_n) e^{ikq_n} + C_2 A(\theta_n) e^{-ikq_n}] & \text{if } x < \zeta \\ -C\sqrt{2\pi}e^{i\frac{\pi}{4}} \displaystyle\sum_{n=0}^{N} \frac{\Psi_n(\eta) e^{ika_n(x_0-\zeta)}}{ka_n\sqrt{k_n}} [C_1 A(\pi+\theta_n) e^{ikq_n} + C_2 A(\pi-\theta_n) e^{-ikq_n}] & \text{if } x > \zeta \end{cases} \tag{A.5}
$$

This result is identical with the one obtained previously.

We also can include in the solution the modes given by Eq. (2.6) that are not propagating in the inner region. Following the same procedure as for the first N modes, the reflection, R_n, and transmission, T_n, coefficients for these modes of the scattered field are determined as:

$$
T_n \sim \frac{i}{2ka_n\sqrt{k_n}} [D_1 e^{kp_0} \cdot A(i\theta_n) + D_2 e^{-kp_0} \cdot A(-i\theta_n)] \tag{A.6}
$$

$$
R_n \sim \frac{i}{2ka_n\sqrt{k_n}} [D_1 e^{kp_0} \cdot A(\pi + i\theta_n) + D_2 e^{-kp_0} \cdot A(\pi - i\theta_n)] \tag{A.7}
$$

To describe the case for which the embedded object is close to the boundary, we assume without loss of generality the boundary to be the top boundary with the

condition $u = 0$ on $z' = 0$. The same method of matched asymptotics can be applied with slight modifications.

The outer solution for both, the scattered field and the Green's function, remains unchanged. We note that $C_2 = -C_1$ in Eq. (2.6) due to the specified top boundary condition. As for the inner problem, it is now analogous to the scattering by an object in the half-space. For the inner problem the scattered far field is given as:

$$u^s \sim C\frac{e^{i\bar{k}n_0\rho}}{\sqrt{\bar{k}\rho}}[\oint_{\partial\Omega}\frac{\partial u}{\partial \nu}e^{i\bar{k}\vec{x}\cdot\hat{r}(\theta)}ds - \oint_{\partial\Omega}\frac{\partial u}{\partial \nu}e^{i\bar{k}\vec{x}\cdot\hat{r}(-\theta)}dse^{2ikh\sin\theta}] \tag{A.8}$$

The angle θ is measured counterclockwise, so we can use the definition of the far-field pattern, given earlier to obtain

$$u^s \sim C\frac{e^{i\bar{k}n_0\rho}}{\sqrt{\bar{k}\rho}}[A(\theta) - A(-\theta)e^{2i\bar{k}h\sin\theta}] \tag{A.9}$$

To match two representations, the inner expansion for the scattered field and the outer expansion for the Green's function are applied on the semicircle of radius $r = \delta$ in the matching region where both are assumed valid. They are used in the integration to determine the matched scattered field

$$u^s(\zeta,\eta) = -\delta\int_{-\alpha}^{\pi+\alpha}(G\frac{\partial u_s}{\partial r} - u_s\frac{\partial G}{\partial r})d\theta \tag{A.10}$$

where angle α is defined by $\sin\alpha = \dfrac{z_0}{\delta} = \dfrac{\epsilon h}{\delta}$.

We make the approximation for $q_0 = \displaystyle\int_0^{z_0}\sqrt{n(s)^2 - a_n^2}\,ds$. Since $z_0 = \epsilon h$ is small, then $q_0 \sim z_0 k_n$, and $kq_0 \sim \bar{k}hn_0\sin\theta_n$, and we find that the unknown coefficients are given by

$$T_n \sim C_1\frac{i\sqrt{2y}e^{i(y-\frac{\pi}{4})}}{8a_n\sqrt{\pi k_n}}[-I_1 + I_2 + I_3 - I_4] \tag{A.11}$$

$$R_n \sim C_1\frac{i\sqrt{2y}e^{i(y-\frac{\pi}{4})}}{8a_n\sqrt{\pi k_n}}[-J_1 + J_2 + J_3 - J_4] \tag{A.12}$$

where

$$I_1 \sim \int_{-\alpha}^{\pi+\alpha}A(\theta)e^{ikq_0}e^{iy(-\cos\theta\cos\theta_n+\sin\theta\sin\theta_n)}(1+\cos\theta\cos\theta_n - \sin\theta\sin\theta_n)d\theta$$

$$
\begin{aligned}
J_1 &\sim \int_{-\alpha}^{\pi+\alpha} A(\theta) e^{ikq_0} e^{iy(\cos\theta\cos\theta_n+\sin\theta\sin\theta_n)}(1-\cos\theta\cos\theta_n-\sin\theta\sin\theta_n)d\theta \\
I_3 &\sim \int_{-\alpha}^{\pi+\alpha} A(\theta) e^{-ikq_0} e^{iy(-\cos\theta\cos\theta_n-\sin\theta\sin\theta_n)}(1+\cos\theta\cos\theta_n+\sin\theta\sin\theta_n)d\theta \\
J_3 &\sim \int_{-\alpha}^{\pi+\alpha} A(\theta) e^{-ikq_0} e^{iy(\cos\theta\cos\theta_n-\sin\theta\sin\theta_n)}(1-\cos\theta\cos\theta_n+\sin\theta\sin\theta_n)d\theta
\end{aligned}
$$

$$
\begin{aligned}
I_2 &\sim \int_{-\alpha}^{\pi+\alpha} A(-\theta) e^{i\bar{k}hn_0(2\sin\theta+\sin\theta_n)-iy(\cos\theta\cos\theta_n-\sin\theta\sin\theta_n)}(1+\cos\theta\cos\theta_n-\sin\theta\sin\theta_n)d\theta \\
J_2 &\sim \int_{-\alpha}^{\pi+\alpha} A(-\theta) e^{i\bar{k}hn_0(2\sin\theta+\sin\theta_n)+iy(\cos\theta\cos\theta_n+\sin\theta\sin\theta_n)}(1-\cos\theta\cos\theta_n-\sin\theta\sin\theta_n)d\theta \\
I_4 &\sim \int_{-\alpha}^{\pi+\alpha} A(-\theta) e^{i\bar{k}hn_0(2\sin\theta-\sin\theta_n)-iy(\cos\theta\cos\theta_n+\sin\theta\sin\theta_n)}(1+\cos\theta\cos\theta_n+\sin\theta\sin\theta_n)d\theta \\
J_4 &\sim \int_{-\alpha}^{\pi+\alpha} A(-\theta) e^{i\bar{k}hn_0(2\sin\theta-\sin\theta_n)+iy(\cos\theta\cos\theta_n-\sin\theta\sin\theta_n)}(1-\cos\theta\cos\theta_n+\sin\theta\sin\theta_n)d\theta
\end{aligned}
$$

To evaluate the integrals asymptotically, we again use the method of stationary phase. However, now we need to consider two cases. In the first case we assume $y\sin\theta_n \gg \bar{k}h = O(1)$. In the second case, we assume $y\sin\theta_n \sim \bar{k}h = O(1)$. After the integration is carried out the reflection, R_n, and transmission, T_n, coefficients are determined as (identical in both cases) :

$$
T_n \sim C_1 \frac{1}{2ika_n\sqrt{k_n}}[e^{ikq_n}\cdot A(-\theta_n) - e^{-ikq_n}\cdot A(\theta_n)] \tag{A.13}
$$

$$
R_n \sim C_1 \frac{1}{2ika_n\sqrt{k_n}}[e^{ikq_n}\cdot A(\pi+\theta_n) - e^{-ikq_n}\cdot A(\pi-\theta_n)] \tag{A.14}
$$

APPENDIX B

SCATTERING IN PEKERIS WAVEGUIDE

The Pekeris waveguide consists of a homogeneous layer over a half-space homogeneous bottom layer, i.e. represents semi-infinite waveguide with piecewise constant index of refraction. The formulation of the problem is similar to given above, except that the bottom boundary condition $B_2(u) = 0$ on $z' = H$ is not given explicitly, but determined from the radiation condition at infinity. Depth of the interface between two layers is given as $H, H \gg L$. We assume that the field, and its normal derivative, multiplied by a constant, are continuous across the interface, and top boundary to be sound soft.

The same method of matched asymptotics is applied for Pekeris waveguide. The values of reflection and transmission coefficients agree with given above (2.14,2.13). Since the Green's function in this case is represented as an integral in a complex plane with a branch cut [6], the contribution to the integral along the cut describes the continuous spectrum. The integrals for the matched scattered field were evaluated by the method of steepest descent, and the continuous spectrum was obtained as $I = IC_1 + IC_2$, where

$$IC_1 = \int_{C1(C1')+C2(C2')} = \frac{1}{2\pi} \int_0^{k_2} \frac{\exp i\alpha|\zeta - x|}{\frac{\lambda_1\rho_2}{\lambda_2\rho_1}\cos\lambda_1{}^2 + \frac{\lambda_2\rho_1}{\lambda_1\rho_2}\sin\lambda_1{}^2} \frac{\sin\lambda_1}{\lambda_1} \cdot \begin{cases} (A(-\Phi)e^{i\lambda_1 z_0} - A(\Phi)e^{-i\lambda_1 z_0})\, d\alpha, & x < \zeta \\ (A(\pi+\Phi)e^{i\lambda_1 z_0} - A(\pi-\Phi)e^{-i\lambda_1 z_0})\, d\alpha, & x > \zeta \end{cases} \tag{B.1}$$

$$IC_2 = \int_{C3(C3')+C4(C4')} = \frac{i}{2\pi} \int_0^{\infty} \frac{\exp(-v|\zeta - x_0|)}{\frac{\lambda_1\rho_2}{\lambda_2\rho_1}\cos\lambda_1{}^2 + \frac{\lambda_2\rho_1}{\lambda_1\rho_2}\sin\lambda_1{}^2} \frac{\sin\lambda_1}{\lambda_1} \cdot \begin{cases} (A(-\frac{\pi}{2}+i\beta)e^{i\lambda_1 z_0} - A(\frac{\pi}{2}-i\beta)e^{-i\lambda_1 z_0})\, dv, & x_0 < \zeta \\ (A(-\frac{\pi}{2}-i\beta)e^{i\lambda_1 z_0} - A(\frac{\pi}{2}+i\beta)e^{-i\lambda_1 z_0})\, dv, & x_0 > \zeta \end{cases} \tag{B.2}$$

In the far field, $|\zeta| \gg 1$, the continuous spectrum integral does not affect the scattered field.

$$I \sim \frac{i}{\pi|\zeta|k_1} \frac{\sin k_1}{\frac{k_1\rho_2}{k_2\rho_1}\cos {\lambda_1}^2 + \frac{k_2\rho_1}{k_1\rho_2}\sin {\lambda_1}^2}(A(-\frac{\pi}{2})e^{ik_1z_0} - A(\frac{\pi}{2})e^{-ik_1z_0}) = O(|\zeta|^{-1}) \quad (B.3)$$

The effects in the near-field of the scatterer are fully described by the continuous spectrum. Therefore, the scattered field is completely determined for the given shape of the submerged object throughout the waveguige.

REFERENCES

1. Y. Xu, "The propagating solution and far-field patterns for acoustic harmonic waves in a finite depth ocean," Applicable Analysis, **35**, pp. 129-151, 1990.

2. R.H. Hackman and G.S. Sammelmann, "Multiple-scattering for a target in a oceanic waveguide," J. Acoust. Soc. Am., **84**, pp. 1813-1825, 1988.

3. M. D. Collins and M. F. Werby, "A parabolic equation model for scattering in the ocean," J. Acoust. Soc. Am., **85**, pp. 1895-1902, 1989.

4. G.V. Norton and M.F. Werby, "A numerical technique to describe acoustical scattering and propagation from an object in a waveguide," J. Appl. Phys., **70**, pp. 4101-4112, 1991.

5. F. Ingenito, " Scattering from an object in a stratified medium," J. Acoust. Soc. Am., **82**, pp. 2051-2059, 1987.

6. W.M. Ewing, W.S. Jardetzky, and F. Press, *Elastic Waves in Layered Media*, McGraw-Hill, NY, 1957.

7. A. Zygmund, *Trigonometric series*, Cambridge Univ. Pr., 1988.

8. D.S. Ahluwalia and J.B. Keller, "Exact and asymptotic representation of the sound field in a stratified ocean," in *Wave Propagation and Underwater Acoustics*, edited by J.B. Keller and J.S. Papadakis, Vol. 70 of *Lecture Notes in Physics*, Springer-Verlag, New York, 1977.

9. D. Colton and R. Kress, *Inverse Acoustic and Electromagnetic Scattering Theory*, 2nd ed., Springer-Verlag, NY, 1998.

10. E.K. Skarsoulis, G.A. Athanassoulis, and U.Send, "Ocean acoustic tomography based on peak arrivals," J. Acoust. Soc. Am., **100**, pp. 797-813, 1996.

11. R. Courant and D. Hilbert, *Methods of mathematical physics*, Wiley Classics, 1989.

12. F.B. Jensen, W.A. Kuperman, M.B. Porter, and H. Scmidt, *Computational ocean acoustics*, AIP Press, NY, 1994.

13. P. Gerstoft, "Inversion of seismoacoustic data using genetic algorithms and a posteriory probability distributions," J. Acoust. Soc. Am., **95**, pp. 770-782, 1994.

14. Z.H. Michalopoulou, H. Martynov, and M. B. Porter, "Simulated annealing and genetic algorithms for broadband source focalization," in *Proceedings of the 3rd European Conference on Underwater Acoustics*, edited by J. S. Papadakis, FORTH-IACM, pp.409-414, 1996.

15. T.C. Yang, "The method of range and depth estimation by modal decomposition," J. Acoust. Soc. Am., **82**, pp. 1736-1745, 1987.

16. E.C. Shang, "An efficient high-resolution method of source localization processing in mode space," J. Acoust. Soc. Am., **86**, pp. 1960-1967, 1989.

17. T.C. Yang and T.W. Yates, "Scattering from an object in a stratified medium. I. Frequency dispertion and active localization," J. Acoust. Soc. Am., **92**, pp. 1003-1019, 1994.

18. R. Kress, "Numerical methods in inverse obstacle scattering with reduced data," in *Proceedings of the 4-th International Conference on Mathematical and Numerical Aspects of Wave Propagation*, edited by John A. DeSanto, SIAM, pp.34-43, 1998.

19. Y. Xu, "An injective far-field pattern operator and inverse scattering problem in a finite depth ocean," Proc. Edinburgh Math., **34**, pp. 295-311, 1991.

20. Y. Xu, "Shape reconstruction from far-field patterns in a stratified ocean environment," *IMA preprint*, 1991.

21. T.C. Yang and T.W. Yates, "Scattering from an object in a stratified medium. II. Extraction of scattering signature," J. Acoust. Soc. Am., **92**, pp. 1020-1031, 1994.

22. C. Rozier, D. Lesselier, T.S. Angell, and R.E. Kleinman, "Shape retrieval of an obstacle immersed in shallow water from single-frequency farfields using a complete family method," Inverse Probs., **13**, pp. 487-508, 1997.

23. T. Scotti and A. Wirgin, "Shape reconstruction using diffracted waves and canonical solutions," Inverse Probs., **11**, pp. 1097-1111, 1995.

24. R.P. Gilbert, T. Scotti, A. Wirgin, and Y.S. Xu, "The unidentified object problem in shallow water," J. Acoust. Soc. Am., **103**, pp. 1320-1327, 1998.

25. P. Cristini and A. Wirgin, "Identification of the size, proportions and location of a soft body of revolution in a shallow-water waveguide," Inverse Probs., **16**, pp. 1727-1739, 2000.

26. T.C. Yang, "Scattering from boundary protuberances and revebration imaging," J. Acoust. Soc. Am., **93**, pp. 231-242, 1993.

27. A. Sarkissian, "Extraction of scattering response from measurements made over long ranges in shallow water," J. Acoust. Soc. Am., **102**, pp. 825-832, 1997.

28. G. Dassios, "Convergent low-frequency expansions for penetrable scatterers," J. Math. Phys., **18**, pp. 126-137, 1977.

29. M.R. Weiss, "Inerse scattering in the geometric-optics limit," J. Opt. Soc. Am., **58**, pp. 1524-1528, 1968.

30. G.A. Kriegsmann, "Acoustic target reconstruction using geometrical optics phase information," IMA J. Appl. Math., **48**, pp. 243-247, 1992.

31. R.M. Lewis, "Physical optics inverse diffraction," IEEE Trans. Antennas Propag., **17**, pp. 308-314, 1969.

32. G.A. Kriegsmann, "The flanged waveguide antenna: Discrete reciorocity and conservation," Wave Motion, **29**, pp. 81-95, 1999.

33. G.A. Kriegsmann and P.G. Petropoulos, "An Approximate method for the study of transverse discontinuities in waveguides," Wave Motion, **13**, pp. 123-131, 1991.

34. A.Q. Howard, "On the mathematical theory of electromagnetic radiation from flanged waveguides," J. Math. Phys., **13**, pp. 482-490, 1972.

35. R.A. Dalrymple, "Water waves past abrupt channel transitions," Appl. Ocean Res., **11**, pp. 170-175, 1989.

36. R.A. Dalrymple and P.A. Martin, "Water waves incident on an infinitely long rectangular inlet," Appl. Ocean Res., **18**, pp. 1-11, 1996.

37. H.Y. Yee, L.B. Felsen, and J.B. Keller, "Ray theory of reflection from the open end of a waveguide," SIAM J. Appl. Math., **16**, pp. 268-300, 1968.

38. G.A. Kriegsmann, "Scattering by large resonant cavity structures," Wave Motion, **30**, pp. 329-344, 1999.

39. S. Walker, "Multi-mode cavity effects on the microwave heating of a ceramic slab," *PhD Thesis*, Department of Applied Mathematics, NJIT, 2001.

40. H. Hudde and U. Letens, "Scattering matrix of a discontinuity with a non rigid walls in a lossless circular duct," J. Acoust. Soc. Am., **78**, pp. 1826-1837, 1985.

41. H. Lamb, *Hydrodynamics*, Dover publications, NY, 1945.

42. B. Noble and J.W. Daniel, *Applied linear algebra*, Prentice-Hall, NJ, 1988.